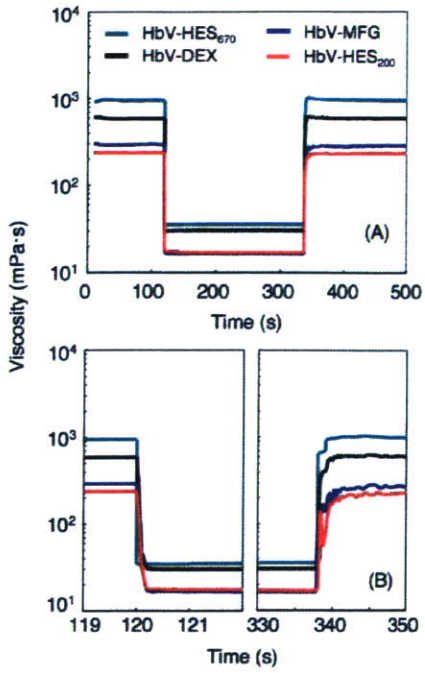

Figure 8. (A) Response of the viscosity of HbV suspended in DEX, HES_{200}, HES_{670}, and MFG to the rapid change in shear rate as measured using the MCR 301 rheometer. The shear rate changed rapidly from 0.1 to 100 s^{-1}; it then returned to 0.1 s^{-1}. The graph is magnified in B. [Hb] = 10 g/dL, 25 °C.

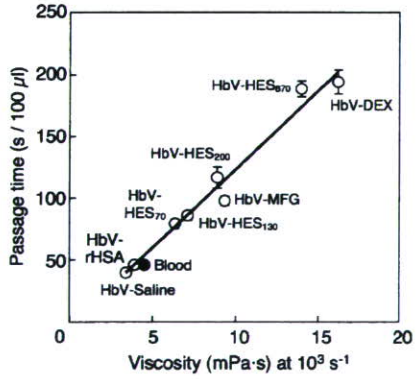

Figure 9. Microchannel flow measurements of HbV suspended in various plasma-substitute solutions and human blood. The time required for the passage of 100 μL of each suspension was plotted against the viscosity at 1000 s^{-1} (from Figure 1). The straight line indicates a linear approximation: $Y = 12.4X$ ($R^2 = 0.9727$). Mean ± SD ($n = 3$).

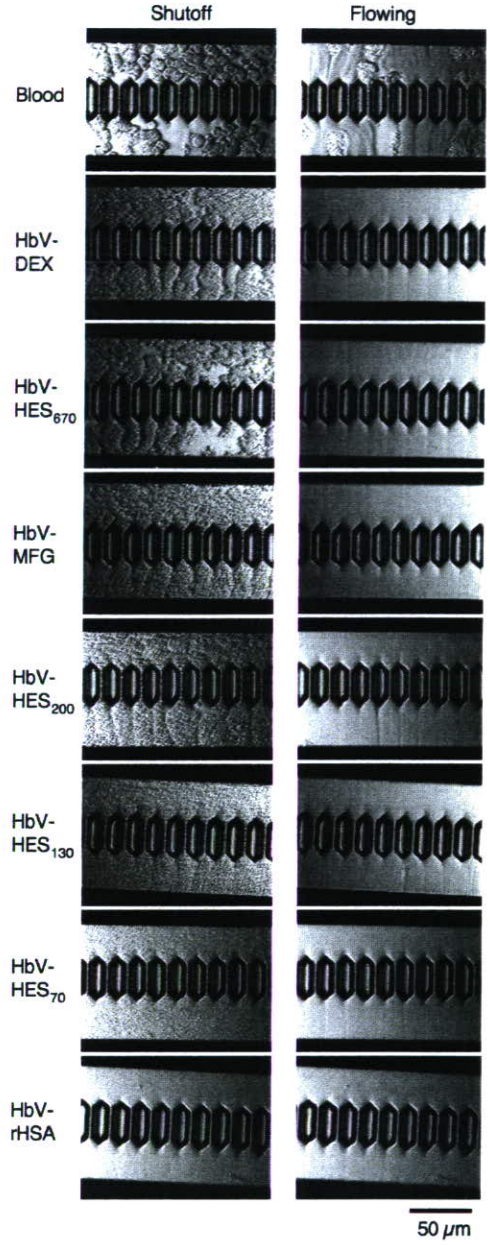

Figure 10. Images of microchannels during the flowing condition and at flow cessation. The direction of flow is from top to bottom. Flocculate formation is apparent at cessation for HbV-DEX, HbV-HES, and HbV-MFG. However, no flocculation was apparent for HbV-rHSA. Under the flowing condition, no plugging of channels occurred for any HbV suspension. However, blood showed partial plugging. In the HES series, a higher-molecular-weight HES shows larger flocculation at cessation.

and the recovery of viscosity that corresponded to flocculate formation was completed within 2 s. Although the responses should depend partially on the sharpness of the shear rate change induced by the motion of the cone plate, these data indicate that the flocculation of HbV is formed rapidly by weak interaction and that it is completely reversible.

Microchannel Flow Measurement. Figure 9 summarizes the relationship between the viscosity of the HbV suspensions at a shear rate of 10^3 s^{-1} and the time required for the passage of 100 μL of the suspensions through the microchannels. The most viscous HbV-DEX required the longest time: 194 ± 10 s. Apparently, a proportional relationship exists between the time required for passage and the fluid viscosity ($R^2 = 0.9727$).

Despite the high viscosities of HbV-DEX, HbV-HES_{670}, HbV-MFG, and HbV-HES_{200}, microscopic observation indicated that no plugging of the microchannels occurred under the flow condition even though clear flocculate formation existed for the cessation of flow (Figure 10). However, stored blood showed the partial plugging of channels even though its viscosity (4.5 mPa·s) and the time required for passage (48 s) were much less than that for HbV suspended in other polymer solutions. At shutoff, HbV-DEX, HbV-MFG, HbV-HES_{200}, and HbV-HES_{670} showed traces of channel flow and phase separation of the suspending medium and flocculation.

Discussion

The results of this study clarified that the HbV suspension has a unique rheological profile from the viewpoint of "suspension rheology." Liposomes are well known to form flocculates or

aggregates in the presence of water-soluble polymers[23,24,40] that were analyzed mainly by turbidity or light-scattering measurements at a very low concentration, where a suspension would consist of a collection of discrete flocculates. However, the HbV suspension consists of a high concentration of HbV with a weight fraction of nearly 16 g/dL in all and a volume fraction of about 40 vol %. Therefore, the flocculated HbV would respond elastically to small deformations, as indicated by the considerable increase in the storage modulus (G') of flocculated suspensions.[25,41] The rheometer that we used (Physica MCR 301) is extremely sensitive to slight shear stress, thereby enabling the detection of subtle rheological changes over a wide range of shear rates ($10^{-4}-10^{3}$ s^{-1}). The RBCs are well known to aggregate reversibly; they are a determinant of the viscoelastic property of non-Newtonian blood because they occupy 40−55% of the blood volume.[33,42] The RBC aggregation, induced by the addition of a water-soluble polymer, influences blood viscosity, hemodynamics, and tissue oxygenation.[43−46] Therefore, it is important to determine the rheological profiles of HbV suspensions as a transfusion alternative.

The HbV suspended in rHSA, a globular protein solution, was a nearly Newtonian fluid. The level of viscosity at higher shear rates was nearly equal to that of human blood. In contrast, HbV suspended in other polymer solutions—HES, DEX, and MFG—showed non-Newtonian properties with a high viscosity at a lower shear rate (shear thinning) because of the flocculation of HbV. A series of HES solutions showed a clear molecular-weight dependence for inducing flocculation. In addition, HbV-HES_{70} showed a similar curve to that of blood. For all combinations of HbV and a polymer solution, the flocculation of HbV should be dissociated at a higher shear rate. Interestingly, the Casson plots show no stress yield for any suspension, probably because the rheometer that we used can measure shear stress values successively, even at extremely low shear rates of 10^{-4} s^{-1}. It is speculated that flocculation formation and dissociation are successive and that no marked critical point exists.

The mechanism of liposome flocculation remains controversial. It is well established in our laboratory that intermacromolecular interactions in water solutions produce macromolecular complexes such as a polyelectrolyte complex and a hydrogen-bonding complex.[47] Therefore, it was plausible that (i) polymer chains would adsorb onto the surfaces of the particles directly to produce bridges.[24] However, it is well known that a PEG aqueous solution and a polysaccharide aqueous solution are immiscible, and it cannot explain the adsorption of DEX and HES on the surface of PEG-modified HbV. Another mechanism was that (ii) the hydration of polymer chains would deflect water molecules from the particles and thereby exclude the particles from the bulk solution.[26] However, this was denied by Meyuhas et al.[23] by the fact that dialysis of liposomes against polymer-containing solutions did not induce aggregation whereas direct addition of the polymer to the liposome solution induced flocculation. Recent practical and theoretical analyses contradict these theories and suggest a depletion mechanism: (iii) A depletion layer develops near a particle surface that is in contact with a polymer solution if the loss of configurational entropy of the polymer coil is not balanced by adsorption energy. Within this layer, the polymer concentration is lower than in the bulk phase. Consequently, as particles approach, the osmotic pressure difference between the interparticle polymer-poor depletion layer and the bulk phase results in solvent displacement into the bulk phase and depletion interaction. Because of this interaction, an attractive force of particles tends to minimize the polymer-poor space between the particles, thereby inducing flocculation.[23,27,48,49]

In the case of depletion interaction, the size of the polymer coil in comparison to interparticle spacing is important. Macromolecules of HES, DEX, and MFG should contain branches; the polymers are more extended or linear than the globular, compact structure of HSA.[50] According to the literature, the radii of gyration (R_g) of these polymers are estimated to be HES_{670} (ca. 19.7 nm), HES_{130} (ca. 12.3 nm),[51] DEX (ca. 8.1 nm),[52] MFG (ca. 10.7 nm),[53] and HSA with the smallest value (ca. 2.8 nm).[54] Even though the R_g of MFG is only half that of HES_{670}, the molar concentration of MFG (1.7 mM), calculated from the concentration and M_n, is about 6 times larger than that of HES_{670} (0.3 mM). It is probable that the more extended polymer chains and the higher molar concentration enhance the exclusion effect from the hydrated sphere of the vesicles, creating a more flocculated vesicle structure. One limitation of this study is that we selected the clinically approved polymer solutions only from a practical point of view. Therefore, the molecular weight distributions are very wide, as indicated by their large M_w/M_n ratios, and their molar concentrations are different. Further analyses are ongoing to clarify the flocculation mechanism using polymers with strictly defined molecular weights and concentrations.

Interestingly, we observed dynamic hysteresis and a shear-thickening profile when the shear rate was increased in the opposite direction for suspensions that showed very high viscosities (HbV-DEX, HbV-HES_{670}, HbV-HES_{200}, and HbV-MFG). These results indicate that the rheological properties of these suspensions are influenced by the time history of the suspension for the growth of flocculation. Typical shear thickening is reported in the case of styrene-methyl acrylate copolymer particles mixed with poly(acrylic acid),[55] which is attributable to the nonlinear elasticity resulting from the entropy of extended bridges and forced desorption caused by hydrodynamic effects. For HbV suspensions, it is speculated that a higher shear rate would extend the distance separating the HbV particles, causing an entropy loss of the solution of polymers with larger R_g, which would cause a regional shear-thickening effect. Another reason would be related to the sedimentation of flocculated HbV, even in the thin solution between the cone and plate. In this case, the concentration of HbV would be lower at the upper layer near the cone, resulting in a slightly lower viscosity at a lower shear rate. With increasing shear rate, the suspension would be homogenized, showing a higher viscosity as a shoulder in Figure 3.

(40) Sou, K.; Endo, T.; Takeoka, S.; Tsuchida, E. *Bioconjugate Chem.* **2000**, *11*, 372−379.
(41) Otsubo, Y. *Heterogeneous Chem. Rev.* **1996**, *3*, 327−349.
(42) Chien, S.; King, R. G.; Skalak, R.; Usami, S.; Copley, A. L. *Biorheology* **1975**, *12*, 341−346.
(43) Freyburger, G.; Dubreuil, M.; Boisseau, M. R.; Janvier, G. *Br. J. Anaesth.* **1996**, *76*, 519−525.
(44) Eckmann, D. M.; Bowers, S.; Stecker, M.; Cheung, A. T. *Anesth. Analg.* **2000**, *91*, 539−545.
(45) Bishop, J. J.; Nance, P. R.; Popel, A. S.; Intaglietta, M.; Johnson, P. C. *Am. J. Physiol. Heart Circ. Physiol.* **2001**, *280*, H222−H236.
(46) Tateishi, N.; Suzuki, Y.; Cicha, I.; Maeda, N. *Am. J. Physiol. Heart Circ. Physiol.* **2001**, *281*, H448−H456.
(47) Tsuchida, E.; Abe, K. *Adv. Polym. Sci.* **1982**, *45*, 1−119.
(48) Neu, B.; Meiselman, H. J. *Biochim. Biophys. Acta* **2006**, *1760*, 1772−1779.
(49) Vincent, B.; Edwards, J.; Emmett, S.; Jones, A. *Colloids Surf.* **1986**, *18*, 261−281.
(50) Takaori, M.; Kobori, M. *Plasma Substitutes and Their Clinical Use*; Kokuseido Publisher: Tokyo, 2004.
(51) Gosch, C. I.; Haase, T.; Wolf, B. A.; Kulicke, W. *Starch* **2002**, *54*, 375−384.
(52) Hirata, Y.; Sano, Y.; Aoki, M.; Shohji, H.; Katoh, S.; Abe, J.; Hitsukuri, S.; Yamamoto, H. *Carbohydr. Polym.* **2003**, *53*, 331−335.
(53) Kaur, M.; Jumel, K.; Hardie, K. R.; Hardman, A.; Meadows, J.; Melia, C. D. *J. Chromatogr., A* **2002**, *957*, 139−148.
(54) Almogren, A.; Furtado, P. B.; Sun, Z.; Perkins, S. J.; Kerr, M. A. *J. Mol. Biol.* **2006**, *356*, 413−431.
(55) Otsubo, Y. *Langmuir* **1999**, *15*, 1960−1965.

The elastic properties of the HbV suspension are readily apparent from the high contribution of the storage modulus (G'). In fact, G' was higher for more viscous HbV suspensions, such as HbV-DEX, HbV-HES_{200}, and HbV-MFG. The strain−sweep measurement clarified that G' decreased gradually with increasing strain. However, G'' was nearly constant at lower strains, and the yielding point for these suspensions was as high as 10% strain. These results indicate that the HbV flocculation structure is not rigid and that reformation occurs easily with subtle strain.

It is speculated that the flocculation of HbV includes interconnected fractal clusters. As shown in Figure 6, both G' and the viscosity increase with increasing concentration of HbV. The logarithmic graph of G' versus ϕ (volume fraction of HbV) shows an almost linear relationship. A theory of Bascall et al.[38] for networks consisting of interconnected fractal clusters predicts $G'-\phi^{3.5\pm0.2}$ for diffusion-limited flocculation and $G'-\phi^{4.5\pm0.2}$ for chemically limited aggregation.[39] For the HbV suspensions, G' varies with ϕ following a power law of order 2.1−2.4 and is much smaller than the theoretical values, supporting the idea that HbV forms fractal clusters through a very weak interaction and that diffusion-limited flocculation is plausible. This also supports the idea that polymer adsorption on the surface of HbV would not involve this system and that the weak interaction enables reversible and rapid flocculation−dissociation in response to the rapid change in shear rates, as shown in Figure 8, and the high yielding point of the stress−sweep measurement in Figure 4.

We reported previously that the surface modification of HbV with PEG prevents aggregation in an HSA solution.[3,18] The amount of PEG is sufficient to prevent aggregation formation in plasma. However, results of the present study show that, even with the PEG modification, HbV undergoes flocculation or aggregation when dispersed into a series of plasma substitutes. Notwithstanding, the flocculation seems not to plug the capillaries, as demonstrated for the first time by microchannel flow experiments. Under a static condition, microscopic observation clearly revealed flocculation. Under the flowing condition in the microchannels, visual observation confirmed the flocculation. However, no plugging was detected in the channels. The time necessary for passage at a perfusion pressure of 20 cmH_2O, which corresponded to an in vivo capillary pressure, was proportional to the fluid viscosity, according to Poiseuille's theory at constant pressure. However, the time required for the passage of blood should depend on the deformability of red blood cells and the activation of platelets and white cells, depending on a pathological condition.[34]

In a living body, perfusion pressure, vascular resistance, and blood viscosity determine organ blood flow. According to Poisseuille's law, increased viscosity reduces flow at a constant applied pressure. For the substitution of a large volume of blood with an HbV suspension as a "transfusion alternative", HbV-rHSA and HbV-HES_{70} with similar viscosity to that of human blood would apparently be appropriate to maintain blood rheology and systemic hemodynamics. It remains to be examined whether other viscous combinations of HbV with DEX, higher-molecular-weight HES, and MFG would be acceptable to a living body. A possible utilization of HbV would be injection at a perioperative hemorrhage. A plasma substitute solution would be injected in an initial phase to maintain blood volume, causing hemodilution, followed by the injection of HbV to maintain O_2 content. This procedure would cause the dilution of both the plasma substitute and HbV. Therefore, the level of HbV flocculation and the viscosity would be reduced somewhat. Actually, we conducted the isovolemic hemodilution of 60% blood volume of rats with the series of plasma substitute solutions and subsequent injection of HbV. The results showed that systemic hemodynamic and respiratory functions were preserved and that no effect of flocculation was evident (unpublished data). The details will be reported elsewhere.

From a physiological point of view, changes in blood viscosity are accompanied by changes in vascular geometry because of autoregulatory processes that are driven by changes in the production of endothelium-derived vasorelaxation factors such as nitric oxide and prostacyclin in response to shear stress on the vascular wall.[56] Progressive hemodilution with a plasma substitute solution decreases blood viscosity, thereby increasing blood flow and vasoconstriction.[57] However, a viscous fluid is advantageous for imparting shear stress on the vascular wall to facilitate the production of vasorelaxation factors and thereby enhance vasorelaxation to improve peripheral blood flow. High blood viscosity is advantageous for transmitting pressure homogeneously to the microvascular network and thereby supplying blood to all capillaries.[58−60] A high-molecular-weight dextran-induced hyperviscosity of blood engenders the dilation of blood vessels.[61] Hemoconcentration increases blood viscosity but reduces vascular resistance.[62] Actually, Erni et al. tested the 40% blood exchange transfusion with HbV suspended in DEX and HES_{200}; they found no capillary plugging. They did find increased plasma viscosity and an improvement of microcirculatory blood flow in ischemic tissues in a hamster skin-flap model.[63−65]

In conclusion, the rheological property of HbV suspension is adjustable to that of human blood through the combination of rHSA and HES_{70}. Other plasma substitutes, such as high-molecular-weight HES, DEX, and MFG, cause HbV flocculation and hyperviscosity. However, reports show that hyperviscosity would not necessarily cause deterioration and in some cases might be advantageous to the body. The combination of HbV and plasma substitute solutions provides a unique opportunity to manipulate the suspension rheology not only as a transfusion alternative but also for other clinical applications such as the oxygenation of ischemic tissues and the ex vivo perfusion system. Further research is necessary to clarify the mechanism of flocculation and the in vivo safety of the combination of HbV and various kinds of plasma substitutes. Projects to collect such data are under way.

Acknowledgment. We acknowledge Dr. Masuhiko Takaori (East Takarazuka Satoh Hospital), Dr. Amy G. Tsai (University of California, San Diego), and Dr. Dominique Erni (Inselspital Hospital, University of Bern) for meaningful discussions related to plasma substitutes and Professor Yasufumi Otsubo (Chiba University) and Mr. N. Hirano (Nihon SiberHegner K.K., Tokyo)

(56) Smiesko, V.; Johnson, P. C. *News Physiol. Sci.* **1993**, *8*, 34−38.
(57) Hudak, M. L.; Jones, M. D., Jr.; Popel, A. S.; Koehler, R. C.; Traystman, R. J.; Zeger, S. L. *Am. J. Physiol. Heart Circ. Physiol.* **1989**, *257*, H912−H917.
(58) Tsai, A. G.; Acero, C.; Nance, P. R.; Cabrales, P.; Frangos, J. A.; Buerk, D. G.; Intaglietta, M. *Am. J. Physiol. Heart Circ. Physiol.* **2005**, *288*, H1730−H1739.
(59) Tsai, A. G.; Intaglietta, M. *Biorheology* **2001**, *38*, 229−237.
(60) de Wit, C.; Schafer, C.; von Bismarck, P.; Bolz, S. S.; Pohl, U. *Pflugers Arch.* **1997**, *434*, 354−361.
(61) Chen, R. Y. Z.; Carlin, R. D.; Simchon, S.; Jan, K. M.; Chien, S. *Am. J. Physiol. Heart Circ. Physiol.* **1989**, *256*, H898−H905.
(62) Martini, J.; Tsai, A. G.; Cabrales, P.; Johnson, P. C.; Intaglietta, M. *Am. J. Physiol. Heart Circ. Physiol.* **2006**, *291*, H310−H317.
(63) Plock, J. A.; Contaldo, C.; Sakai, H.; Tsuchida, E.; Leunig, M.; Banic, A.; Menger, M. D.; Erni, D. *Am. J. Physiol. Heart Circ. Physiol.* **2005**, *289*, H2624−H2631.
(64) Contaldo, C.; Plock, J.; Sakai, H.; Takeoka, S.; Tsuchida, E.; Leunig, M.; Banic, A.; Erni, D. *Crit. Care Med.* **2005**, *33*, 806−812.
(65) Contaldo, C.; Schramm, S.; Wettstein, R.; Sakai, H.; Takeoka, S.; Tsuchida, E.; Leunig, M.; Banic, A.; Erni, D. *Am. J. Physiol. Heart Circ. Physiol.* **2003**, *285*, H1140−1147.

for discussions of technical problems pertaining to viscoelastic measurements. The rHSA, HES, and MFG used in this study were gifts from Nipro Co., Fresenius Kabi A.G., and B. Braun, respectively. This study was supported by Health and Labour Sciences Research Grants (Research on the Regulatory Science of Pharmaceuticals and Medical Devices), the Ministry of Health, Labour and Welfare, Japan (H.S., E.T.), Grants-in-Aid for Scientific Research from the Japan Society for the Promotion of Science (B16300162) (H.S.), and Oxygenix Inc. (Tokyo, Japan). H.S., S.T., and E.T. are consultants of Oxygenix Inc.

Supporting Information Available: Viscosity of plasma-substitute solutions. This material is available free of charge via the Internet at http://pubs.acs.org.

LA7004503

THE JOURNAL OF BIOLOGICAL CHEMISTRY VOL. 283, NO. 3, pp. 1508–1517, January 18, 2008

Encapsulation of Concentrated Hemoglobin Solution in Phospholipid Vesicles Retards the Reaction with NO, but Not CO, by Intracellular Diffusion Barrier*

Received for publication, September 12, 2007, and in revised form, November 13, 2007 Published, JBC Papers in Press, November 14, 2007, DOI 10.1074/jbc.M707660200

Hiromi Sakai[‡], Atsushi Sato[§], Kaoru Masuda[¶], Shinji Takeoka[§1], and Eishun Tsuchida[‡2]

From the [‡]Research Institute for Science and Engineering and [§]Graduate School of Advanced Science and Engineering, Waseda University, Tokyo 169-8555, Japan and [¶]Kobelco Research Institute, Inc., Kobe 651-2271, Japan

One physiological significance of the red blood cell (RBC) structure is that NO binding of Hb is retarded by encapsulation with the cell membrane. To clarify the mechanism, we analyzed Hb-vesicles (HbVs) with different intracellular Hb concentrations, $[Hb]_{in}$, and different particle sizes using stopped-flow spectrophotometry. The apparent NO binding rate constant, $k'_{on}{}^{(NO)}$, of HbV at $[Hb]_{in}$ = 1 g/dl was 2.6 × 10^7 M^{-1} s^{-1}, which was almost equal to $k_{on}{}^{(NO)}$ of molecular Hb, indicating that the lipid membrane presents no obstacle for NO binding. With increasing $[Hb]_{in}$ to 35 g/dl, $k'_{on}{}^{(NO)}$ decreased to 0.9 × 10^7 M^{-1} s^{-1}, which was further decreased to 0.5 × 10^7 M^{-1} s^{-1} with enlarging particle diameter from 265 to 452 nm. For CO binding, which is intrinsically much slower than NO binding, $k'_{on}{}^{(CO)}$ did not change greatly with $[Hb]_{in}$ and the particle diameter. Results obtained using diffusion simulations coupled with elementary binding reactions concur with these tendencies and clarify that NO is trapped rapidly by Hb from the interior surface region to the core of HbV at a high $[Hb]_{in}$, retarding NO diffusion toward the core of HbV. In contrast, slow CO binding allows time for further CO-diffusion to the core. Simulations extrapolated to larger particles (8 μm) showing retardation even for CO binding. The obtained $k'_{on}{}^{(NO)}$ and $k'_{on}{}^{(CO)}$ yield values similar to those reported for RBCs. In summary, the intracellular, not extracellular, diffusion barrier is predominant due to the rapid NO binding that induces a rapid sink of NO from the interior surface to the core, retarding further NO diffusion and binding.

Physicochemical analyses of O_2 uptake and release behaviors of red blood cells (RBCs)[3] have revealed that the cellular structure retards all reactions in comparison with the homogeneous cell-free Hb solution (1–5). However, nature has selected this cellular structure through evolution. Reasons for Hb encapsulation in RBCs are as follows: (i) decreases in a high colloidal osmotic pressure of an Hb solution; (ii) prevention of removal of Hb from blood circulation through renal gloreruli; (iii) preservation of the chemical environment in cells, such as the concentrations of electrolytes (phosphates, 2,3-diphosphoglyceric acid, ATP, etc.) and many enzymes; and (iv) modulation of entrapment of endogenous gaseous messenger molecules (NO and CO) (6, 7) because it has been clarified in pathological conditions with hemolysis (8) and in the development of some Hb-based oxygen carriers (HBOCs) (9–16) that entrapment of endothelium-derived NO induces vasoconstriction, hypertension, reduced blood flow, and vascular damage. CO is also a vasorelaxation factor, especially in hepatic microcirculation (17). Entrapment of CO by a cell-free Hb solution induces constriction of sinusoidal capillaries (18). These side effects of molecular Hb imply the importance of the cellular structure of RBC.

Despite such a background in this field, the mechanism of retardation of NO binding by Hb encapsulation in RBC remains controversial (19–21). It remains unclear whether (i) an unstirred layer is formed as an extracellular diffusion barrier surrounding the RBC (6, 9); (ii) a protein-rich RBC cytoskeletal submembrane becomes a physical barrier against NO diffusion (22, 23); or (iii) gas diffusion is retarded because of the viscous Hb solution in RBC (2). As chemists, it seems to us that these controversies are attributable to the complex and fragile structure of RBC and chemically unstable NO, which make it difficult to analyze the binding rate constant of NO to RBC.

Hemoglobin-vesicles (HbVs) or liposome- encapsulated Hbs have been developed as transfusion alternatives. Their efficacy as O_2 carriers is comparable with that of RBC (24–28). It has been thought that liposomes as a molecular assembly are a fragile capsule. However, appropriate lipid composition and polyethylene glycol modification on the surface of vesicles stabilize the dispersion state (29) and enable stopped-flow measure-

* This work was supported in part by Health and Labor Sciences Research Grants (Research on Regulatory Science of Pharmaceuticals and Medical Devices), Ministry of Health, Labor, and Welfare, Japan (to H. S. and E. T.) and by Grants-in-Aid for Scientific Research from the Japan Society for the Promotion of Science B16300162 (to H. S.) and 18500368 (to S. T.), and Global COE "Practical Chemical Wisdom" (to S. T.). The costs of publication of this article were defrayed in part by the payment of page charges. This article must therefore be hereby marked "*advertisement*" in accordance with 18 U.S.C. Section 1734 solely to indicate this fact.

[1] Present address: Consolidated Research Institute for Advanced Science and Medical Care, Waseda University, 3-4-1 Okubo, Shinjuku, Tokyo 169-8555, Japan.

[2] To whom correspondence should be addressed: Research Institute for Science and Engineering, Waseda University, 3-4-1 Okubo, Shinjuku, Tokyo 169-8555, Japan. Tel.: 81-3-5286-3120; Fax: 81-3-3205-4740; E-mail: eishun@waseda.jp.

[3] The abbreviations used are: RBC, red blood cell; Hb, hemoglobin; metHb, methemoglobin; deoxyHb, deoxyhemoglobin; HbV, hemoglobin-vesicles; $[Hb]_{in}$, intracellular Hb concentration; $[heme]_{in}$, intracellular heme concentration; k_{on}, binding rate constant of elementary reaction; $k'_{on}{}^{(NO)}$, apparent NO binding rate constant; $k'_{on}{}^{(CO)}$, apparent CO binding rate constant; HBOC, Hb-based oxygen carrier; P_{50}, oxygen partial pressure at which Hb is half-saturated; D_{Hb}, diffusion constant of Hb; D_{O_2}, diffusion constant of O_2; D_{NO}, diffusion constant of NO; D_{CO}, diffusion constant of CO.

ments without causing hemolysis (26, 30). Although stopped-flow measurement is becoming classical, it allows accurate measurement of the binding rate constant of ligands (31). HbV is a molecular assembly composed of lipids and a concentrated Hb solution (32), and its physicochemical properties can be regulated easily (33–35) to elucidate their influences on the ligand binding profiles. In this paper, we describe analyses of the influences of intracellular Hb concentration, $[Hb]_{in}$, and the particle size of HbV on the apparent binding rate constants of NO and CO. Moreover, we attempted computer simulations to recreate the phenomena, clarify the underlying mechanism, and predict the ligand binding profiles of larger particles, such as RBCs.

TABLE 1

Physicochemical characterization of a series of HbV prepared for the stopped flow spectrophotometry to observe the NO and CO binding profiles

Samples 1–4 were used to examine the influence of intracellular Hb concentration ($[Hb]_{in}$). Samples 4–6 were used to study the influence of particle diameter. The P_{50} value (oxygen tension at which Hb is half-saturated with oxygen) were regulated in the narrow range of 13–16 torrs to minimize the influence of Hb allostery on the binding rate constants of NO and CO.

Sample entry number	$[Hb]_{in}$	Particle size	P_{50}
	g/dl	*nm*	*torrs*
1	1	305 ± 105	13
2	10	277 ± 103	15
3	20	278 ± 94	15
4	35	265 ± 57	14
5	35	178 ± 74	16
6	35	452 ± 184	14

EXPERIMENTAL PROCEDURES

Preparation of Hb Solution and Hb-vesicles with Various $[Hb]_{in}$—A concentrated human carbonylhemoglobin solution (40 g/dl, desalted) was obtained through purification from outdated donated blood provided by the Japanese Red Cross Society (Tokyo, Japan), as reported previously (36, 37). This was diluted by 10 times with a phosphate-buffered saline (PBS) solution (pH 7.4; Wako Pure Chemical Industries Ltd., Tokyo). It was then concentrated again to 40 g/dl using an ultrafiltration (cut-off M_r 10,000; Advantec, Tokyo) at 4 °C. This solution was diluted to 1, 10, 20, and 35 g/dl using the same PBS solution. They were used for preparation of HbV with different $[Hb]_{in}$. The viscosities of these Hb solutions were measured using a rheometer (Physica MCR 301; Anton Paar GmbH, Graz, Austria) as 0.9, 1.1, 2.1, and 10.1 centipose, respectively, at 10 s^{-1} and 25 °C. In this experiment, we added no allosteric effector, such as an organic phosphate, because we intended to compare the Hb solution and HbV with different $[Hb]_{in}$ at the same O_2 affinity (P_{50}, oxygen partial pressure at which Hb is half-saturated). A linear relationship exists between P_{50} and NO affinity of Hb (38). In the present study, P_{50} was regulated solely using Cl^- and phosphate of PBS (35). The lipid bilayer comprised 1,2-dipalmitoyl-*sn*-glycero-3-phosphatidylcholine, cholesterol, 1,5-*O*-dihexadecyl-*N*-succinyl-L-glutamate (Nippon Fine Chemical Co. Ltd., Osaka, Japan), and 1,2-distearoyl-*sn*-glycerol-3-phosphatidylethanolamine-*N*-polyethylene glycol 5000 (NOF Corp., Tokyo, Japan) at a molar composition of 5/5/1/0.033. It is reported that unsaturated phospholipids are susceptible to lipid peroxidation and induce Hb denaturation (39, 40). Hb interacts with such a liposomal membrane and converts to metHb, leading synergistically to the heme loss and lipid peroxidation. Unsaturated fatty acid is susceptible to nitration (41). However, we use saturated phospholipids that essentially do not induce such reactions (39, 40, 42). The mean particle diameter was regulated by an extrusion method to 265–305 nm to study the influence of $[Hb]_{in}$, and to 178, 265, and 452 nm at the same $[Hb]_{in}$ (equal to 35 g/dl) to study the influence of the particle diameter (32, 34, 43, 44) (Table 1). After removing the unencapsulated Hb solution using ultracentrifugation, HbV was resuspended in the same PBS solution (pH 7.4) at [heme] = 300 μM. Therefore, the carbonylhemoglobin in HbV is converted to HbO_2 by photodissociation of CO by illuminating visible light under O_2 atmosphere. Briefly, an aliquot of CO-bound HbV was put in a glass flask; this was rotated using a rotary evaporator while the flask was immersed in cold water and illuminated using a halogen lamp (500 watts) with a continuous and gentle O_2 flow inside the flask for several minutes. The complete conversion to HbO_2 was confirmed by absorption spectroscopy in the Q band. The physicochemical characteristics of the obtained HbVs are listed in Table 1. The particle size distribution was measured using a dynamic light-scattering method (Submicron Particle Size Analyzer, model N4 PLUS; Beckman-Coulter, Inc., Fullerton, CA). The P_{50} values were obtained from the oxygen equilibrium curve measured with a Hemox-Analyzer (TCS Medical Science, Philadelphia, PA); all samples were ~13–16 torrs at 37 °C.

Stopped-flow Analyses—The time course of the ligand binding was analyzed at a rapid mixing of a deoxygenated HbV solution and a NO-containing or CO-containing solution using a stopped-flow rapid scan spectrophotometer (model RSP-1000; Unisoku Co. Ltd., Osaka, Japan). Solutions in the two reservoirs (A and B) are mixed rapidly with an applied pressure of 0.3–0.6 megapascals and a dead time for mixing of <1.5 ms. All measurements were performed at 25 °C. A PBS solution (3 ml each) was poured into both reservoirs and sealed using septum rubber seals. The reservoirs were deoxygenated by N_2 bubbling for over 30 min for the complete removal of O_2. This is important in the case of NO bubbling to prevent the NO loss and metHb formation. The HbV stock solution (~30 μl, [heme] = 300 μM) was injected into Reservoir A to adjust [heme] finally to 3 μM; the N_2 bubbling was changed to flowing to avoid denaturation of the solutes. Complete deoxygenation was confirmed using preliminary stopped-flow measurements (wavelength: 385–593 nm), where the Soret band showed a maximum absorption (λ_{max}) at 430 nm attributable to the presence of deoxyHb. In Reservoir B, NO or CO gas bubbling was started; a gentle N_2 flowing was maintained in Reservoir A. The mixed gases for NO binding (NO, 0.2029%; N_2, 99.7971%) and for CO binding (CO, 14.14%; N_2, 85.86%) were purchased from Takachiho Chemical Industrial Co., Ltd. (Tokyo). After about 10 min of bubbling, stopped flow measurement was initiated. The sampling interval and the exposure time were set as 1 ms. The measurement time was 210 ms. All measurements were performed three times, and the change of absorbance at 430 nm was plotted as a function of time. The apparent binding rate constants of NO and CO ($k'_{on}{}^{(NO)}$, and $k'_{on}{}^{(CO)}$, respectively) were calculated using Equation 1 under the assumption of homogeneous distribution

of Hb, irreversible second order reaction, and pseudo-first-order reaction when gas molecules are abundant,

$$\ln\frac{\Delta A_t}{\Delta A_0} = -k'_{on} \cdot C_{Gas} \cdot t \qquad \text{(Eq. 1)}$$

where ΔA_t represents the change of absorbance at 430 nm at time t (equal to $A_t - A_{t=\infty}$), and ΔA_0 is the absorbance at the initial time (equal to $A_{t=0} - A_{t=\infty}$). C_{Gas} is the initial gas concentration. In the case of the NO binding experiment, NO (1.9 μM) is not excessively abundant in comparison with heme concentration (1.5 μM); therefore, we calculated the apparent binding rates from the slopes of the initial phase of reactions.

Computer Simulation—We assumed that HbV is spherical and dispersed homogeneously. The gas diffusion constants are much larger than those of Hb molecule (7 nm) and HbV (250 nm) (45). Accordingly, we analyzed only gas diffusion and the formation of ligand-bound Hb in a single HbV particle. We did not consider the extracellular diffusion barrier because of the rapid mixing of small particles, and also we did not consider the gas permeability constant in the lipid bilayer, because the thickness of the lipid bilayer (~5 nm) is thin in comparison with the particle diameter. (Our results show that they would not be important parameters in our system.) To simplify the equation, the distance from the surface to the core of HbV, 125 nm, was divided by 12.5 nm into 10 units. For simulation of a larger particle, such as that with an 8000-nm diameter, 4000 nm was divided by 12.5 nm into 320 units. The first unit is located at the HbV surface and is in the concentration boundary condition. The last unit is located in the core of HbV in the closed condition. From the gas diffusion equation (Equation 2), the one-dimensional diffusion from the surface to the core of the particle can be expressed as Equation 3,

$$\frac{\partial C_{Gas}}{\partial t} = D\frac{\partial^2 C_{Gas}}{\partial x^2} \qquad \text{(Eq. 2)}$$

$$\Delta C_{Gas}(t_i, x_j) = D \cdot \left(\frac{-A_j \cdot (C_{Gas}(t_i, x_j) - C_{Gas}(t_i, x_{j-1})) + A_{j+1} \cdot (C_{Gas}(t_i, x_{j+1}) - C_{Gas}(t_i, x_j))}{V_j \cdot \Delta x}\right) \cdot \Delta t \qquad \text{(Eq. 3)}$$

where $C_{Gas}(t_i, x_j)$ represents the gas concentration at time i (t_i) in 1 unit (x_j; distance from the surface of HbV); $\Delta C_{Gas}(t_i, x_j)$ is a mass change by diffusion; A_j is the interface area of the units $j - 1$ and j, and it changes with the distance from the core of HbV; Δt is the step time; V_j is the volume of the unit j; and Δx is the distance between neighboring units. A gas molecule reacts with a heme in Hb. We assumed that the reaction is irreversible. Therefore, the changes of concentrations are expressed as Equations 4 and 5 with a binding rate constant, k_{on}, of an elementary gas binding reaction.

$$\frac{dC_{heme}}{dt} = -k_{on} \cdot C_{Gas} \cdot C_{heme} \qquad \text{(Eq. 4)}$$

$$\frac{dC_{Gas}}{dt} = \frac{dC_{heme}}{dt} \qquad \text{(Eq. 5)}$$

At a step time Δt and in a step unit Δx, the changes of concentrations (ΔC_{heme}, $\Delta C'_{Gas}$) by the gas bindings are expressed as Equations 6 and 7.

$$\Delta C_{heme}(t_i, x_j) = -k_{on} \cdot C_{Gas}(t_i, x_j) \cdot C_{heme}(t_i, x_j) \cdot \Delta t \qquad \text{(Eq. 6)}$$

$$\Delta C'_{Gas}(t_i, x_j) = -k_{on} \cdot C_{Gas}(t_i, x_j) \cdot C_{heme}(t_i, x_j) \cdot \Delta t \qquad \text{(Eq. 7)}$$

At the onset of reaction by mixing two solutions in the stopped-flow apparatus, the gas diffuses into the HbV. Therefore, the initial unbound free gas concentration inside the vesicle is assumed to be zero. The initial unbound free heme concentrations of HbV are 620–21,700 μM ($[Hb]_{in}$ = 1–35 g/dl); they decrease with the reactions of gas molecules. All initial values for calculations are summarized in Table 2. The diffusion constant of the Hb molecule is concentration-dependent and decreases from 77 to 7.4 $\mu m^2 s^{-1}$ with increasing $[Hb]_{in}$ from 1 to 35 g/dl (46–48). The diffusion constants of gases are 2 orders larger than that of Hb. The diffusion constant of O_2 in Hb solutions (D_{O_2}) decreases with increasing Hb concentration. The diffusion constants of CO and NO (D_{NO} and D_{CO}, respectively) are calculated from D_{O_2} using Equation 8 (2),

$$D_x = D_{O_2} \cdot \left(\frac{32}{MW_x}\right)^{1/2} \qquad \text{(Eq. 8)}$$

where MW_x is the molecular weight of NO or CO.

One-dimensional diffusion simulation coupled with gas binding reactions was performed based on the equations given above (Equations 3, 6, and 7) according to the finite differential method using a Visual Basic Language Programming (Excel, Microsoft Corp., Japan, Tokyo) in a personal computer. Both C_{Gas} and C_{heme} at t_i were calculated using those at t_{i-1}. Both ΔC_{heme} and $\Delta C'_{Gas}$ were calculated using Equations 6 and 7. Gas molecules diffuse depending on a concentration gradient, and the obtained ΔC_{Gas} of Equation 3 was combined with $\Delta C'_{Gas}$ of Equation 7 for the next step calculation of C_{Gas}. The time interval, Δt, was set as 0.01 μs, and 10^7 steps were required to calculate the reaction profile for 100 ms in the case of HbV with a 250-nm diameter. The data were output at every 5 ms.

As the reaction proceeds, the concentration of gas in the bulk solution decreases. To reflect this, Equation 9 is used,

TABLE 2
Parameters for computer simulations for each HbV with different $[Hb]_{in}$

Parameters	Values			
Diameter (nm)	50, 100, 200, 250, 500, 1000, 2000, 8000			
[heme] in solution (μM)	1.5			
Initial [NO] in solution (μM)	1.9			
Initial [CO] in solution (μM)	67.5			
$k_{on}^{(NO)}$ ($M^{-1} s^{-1}$)	2.7×10^7			
$k_{on}^{(CO)}$ ($M^{-1} s^{-1}$)	3.4×10^6			
	1 g/dl $[Hb]_{in}$	10 g/dl $[Hb]_{in}$	20 g/dl $[Hb]_{in}$	35 g/dl $[Hb]_{in}$
$[heme]_{in}$ (μM)	620	6200	12400	21700
D_{Hb} in HbV ($\mu m^2 s^{-1}$)	77	53	29	7.4
D_{NO} in HbV ($\mu m^2 s^{-1}$)[a]	2080	1590	1160	706
D_{CO} in HbV ($\mu m^2 s^{-1}$)[a]	2150	1640	1200	731

[a] D_{NO} in saline is 2210 $\mu m^2 s^{-1}$ and D_{CO} in saline is 2290 $\mu m^2 s^{-1}$. D_{Hb} in HbV is much smaller than D_{NO} and D_{CO}. For that reason, we did not use D_{Hb} in computer simulations. Consequently, we did not consider the so-called "facilitated gas diffusion" attributable to the diffusion and dissociation of HbNO or HbCO because of the low D_{Hb} and the significantly large equilibrium constants of HbNO and HbCO in comparison with that of HbO_2.

$$C_2(\text{Gas}) = \frac{C_0(\text{Gas}) - C_1(\text{GasTotal}) \cdot \left(\frac{C_0(\text{heme})}{C_1(\text{heme})}\right)}{\left(1 - \frac{C_0(\text{heme})}{C_1(\text{heme})}\right)} \quad \text{(Eq. 9)}$$

where the following variables are used. C_0(Gas) is the initial gas concentration; C_2(Gas) is at the boundary condition (in the bulk solution); C_1(GasTotal) is the sum of the bound and unbound gas molecules in HbV; C_o(heme) is the total heme concentration in the solution (1.5 μM); and C_1(heme) is the heme concentration in HbV (such as 21,700 μM at $[\text{Hb}]_{in}$ = 35 g/dl).

The level of unbound free heme, R, can be expressed as Equation 10, which is used to calculate the levels of reactions for 100 ms and the apparent rate constants from the initial slopes (5 ms).

$$R = \frac{\sum_j V_j \cdot C_{\text{heme}}(t_i, x_j)}{\sum_j V_j \cdot C_{\text{heme}}(t_0, x_j)} \quad \text{(Eq. 10)}$$

RESULTS

NO Binding and CO Binding Profiles of HbV Using Stopped-flow Spectrophotometry—The complete deoxygenation of HbV was clearly confirmed according to the characteristic wavelength of the maximum absorption (λ_{max}) at 430 nm. Because of the strong light-scattering effect of the HbV suspension in comparison with Hb solution and RBC (49), the absorption peaks in the Q band region were not clear in this measurement. After rapid mixing with NO, the immediate absorbance reduction at 430 nm and the increase at 418 nm that correspond to the formation of nitrosylhemoglobin were confirmed (Fig. 1). In the case of mixing with CO, the immediate absorption increase at 419 nm was confirmed. The change of absorption at 430 nm in both reactions was single exponential and indicative of the formation of nitrosylhemoglobin or carbonylhemoglobin in the vesicles.

Time Courses of NO Binding and CO Binding to HbV with Various $[Hb]_{in}$—The scans of spectrophotometry in Fig. 1 were performed three times, and the average level of reaction was plotted as a ratio of absorbance at 430 nm (ΔA_t) at time t, to the initial absorbance (ΔA_0) at time 0 (Fig. 2). The *graph* shows that the NO binding is retarded with increasing $[\text{Hb}]_{in}$ from 1 to 35 g/dl. However, no such change was observed in the case of CO binding. From the slopes shown in Fig. 2, the apparent binding rate constants of $k'_{on}{}^{(NO)}$ for NO and $k'_{on}{}^{(CO)}$ for CO were obtained according to Equation 1 and were plotted against $[\text{Hb}]_{in}$ (Fig. 3*A*). This clearly shows that $k'_{on}{}^{(NO)}$ is dependent on $[\text{Hb}]_{in}$; it decreases from 2.6×10^7 to 0.9×10^7 $\text{M}^{-1}\,\text{s}^{-1}$ with increasing $[\text{Hb}]_{in}$ from 1 to 35 g/dl. It must be emphasized that $k'_{on}{}^{(NO)}$ at $[\text{Hb}]_{in}$ = 1 g/dl was almost identical to $k_{on}{}^{(NO)}$ of a cell-free Hb solution (2.7×10^7 $\text{M}^{-1}\,\text{s}^{-1}$). On the other hand, $k'_{on}{}^{(CO)}$ values at $[\text{Hb}]_{in}$ = 1 and 35 g/dl were 3.1×10^5 and 3.0×10^5 $\text{M}^{-1}\,\text{s}^{-1}$, respectively, and almost identical at any $[\text{Hb}]_{in}$ and even to $k_{on}{}^{(CO)}$ of a cell-free Hb solution.

Time Courses of NO Binding and CO Binding to HbV with Different Particle Sizes—The influence of particle size was investigated. At the same $[\text{Hb}]_{in}$ (35 g/dl), HbVs with different particle sizes were prepared. As shown in Fig. 3*B*, $k'_{on}{}^{(NO)}$ decreased from 1.5×10^7 $\text{M}^{-1}\,\text{s}^{-1}$ to 6.5×10^6 $\text{M}^{-1}\,\text{s}^{-1}$ with increasing the diameter from 178 ± 74 to 452 ± 184 nm. On the other hand, CO binding showed no such remarkable changes.

Computer Simulations of NO Binding and CO Binding to HbV—Computer simulations of the experimental results of NO and CO bindings to HbV at different $[\text{Hb}]_{in}$ (1–35 g/dl) and different particle diameters (50, 100, 200, 250, and 500 nm) were performed, and the obtained $k'_{on}{}^{(NO)}$ and $k'_{on}{}^{(CO)}$ were plotted on Fig. 3. It was clearly recreated that the NO binding is influenced significantly by $[\text{Hb}]_{in}$ and the particle size. Although there were deviations from the experimental results, the NO binding was retarded with increasing $[\text{Hb}]_{in}$ from 1 to 35 g/dl. On the other hand, no such change existed in the case of CO binding, and the simulations fit well with the experimental results (Fig. 3*A*). The

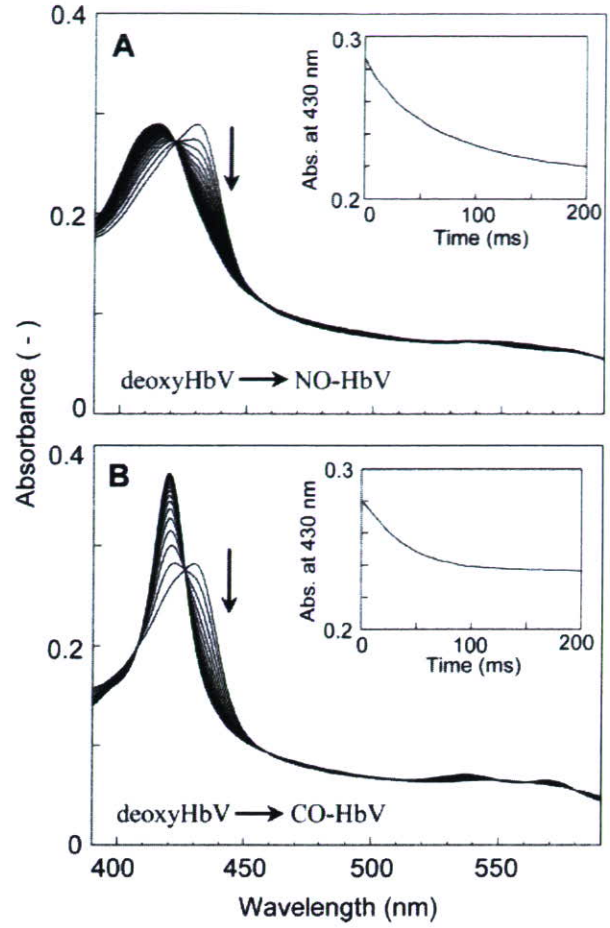

FIGURE 1. **Representative profiles of the reactions of NO or CO with deoxygenated HbV ($[\text{Hb}]_{in}$ = 35 g/dl) using stopped-flow spectrophotometry.** *A*, a NO-bubbled PBS ([NO] = 3.8 μM) and HbV in PBS ([heme] = 3.0 μM) were mixed rapidly using a stopped-flow spectrophotometer; the absorption spectra were collected every millisecond over 0.2 s after mixing. In this figure, the spectroscopic curves of every 10 ms are selected. This *panel* shows clearly that the spectrum of deoxyHbV is mostly converted to NO-HbV in 0.2 s. *Inset*, the time course of the measured absorbance at 430 nm. *B*, a CO-bubbled PBS ([CO] = 135 μM) and HbV in PBS ([heme] = 3.0 μM) were mixed rapidly using a stopped-flow spectrophotometer; the absorption spectra were collected every millisecond over 0.2 s after mixing. In this *panel*, the spectroscopic curves of every 10 ms were selected. This *panel* clearly shows that the spectrum of deoxyHbV is mostly converted to CO-HbV in 0.2 s. *Inset*, the time course of the measured absorbance at 430 nm. The optical path length was 1 cm. All of the experiments were performed at 25 °C.

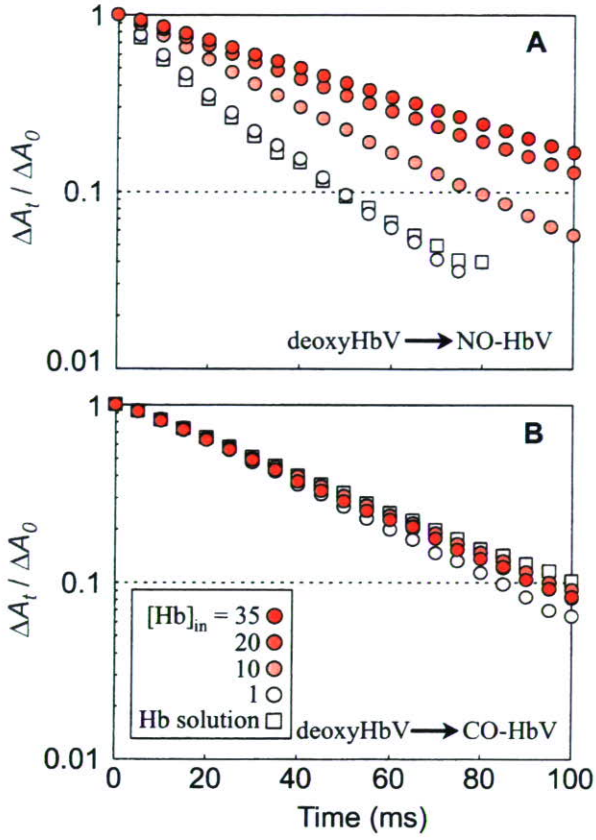

FIGURE 2. **Time courses of NO binding and CO binding by deoxygenated HbV with various [Hb]$_{in}$.** A NO-bubbled PBS (3.8 μM) (*A*) or a CO-bubbled PBS (135 μM) (*B*) and HbVs in PBS ([heme] = 3.0 μM) were mixed rapidly using a stopped-flow spectrophotometer. [Hb]$_{in}$ varies from 1 to 35 g/dl ([heme] = 620–21700 μM); thus, the number of particles differs at the constant [heme] (3.0 μM) in each solution. The level of reaction was plotted on a semilogarithmic *graph* as a ratio of absorption at 430 nm (ΔA_t) at time *t*, to the initial absorption (ΔA_0) at time 0. The results of the cell-free Hb solutions are also plotted, which are almost identical with those of HbV at [Hb]$_{in}$ = 1 g/dl. The *graph* shows that the NO binding rate is retarded with increasing [Hb]$_{in}$ in *A*. However, such a change was not apparent in the case of CO binding in *B*. All of the experiments were performed at 25 °C.

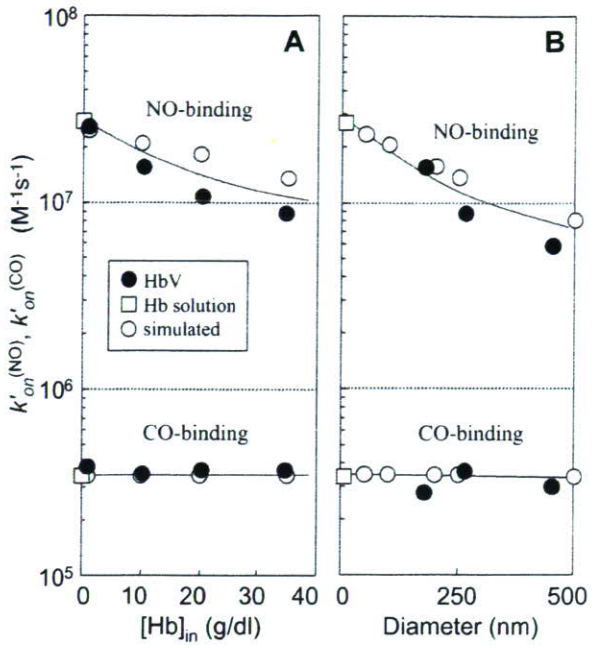

FIGURE 3. **Apparent binding rate constants of NO ($k'_{on}^{(NO)}$) and CO ($k'_{on}^{(CO)}$) of experimental results and computer simulations.** *A*, plotted against [Hb]$_{in}$ of HbV; *B*, plotted against particle diameter. *A*, the apparent binding rate constants (experimental) were calculated from the slopes in Fig. 2. Values of the exact $k_{on}^{(NO)}$ and $k_{on}^{(CO)}$ of the elementary reactions of cell-free Hb solution are also plotted on the *vertical axis*. Those of computer simulations (diameter, 250 nm) are plotted as *open circles*. *B*, the apparent binding rate constants were calculated similarly and plotted against the particle diameter. Values of the exact $k_{on}^{(NO)}$ and $k_{on}^{(CO)}$ of cell-free Hb solution (diameter, 7 nm) were also plotted. Those of computer simulations (diameter, 50, 100, 200, 250, and 500 nm) at [Hb]$_{in}$ = 35 g/dl are plotted as *open circles*. Both *graphs* show that computer simulations recreate well the tendencies of the experimental results; $k'_{on}^{(NO)}$ decreases considerably with increasing [Hb]$_{in}$ and diameter, and $k'_{on}^{(CO)}$ does not show such changes.

size dependence of $k'_{on}^{(NO)}$ and the independence of $k'_{on}^{(CO)}$ were also recreated well as shown in Fig. 3*B*. The larger particle showed a slower rate of NO binding but not CO binding. It should be noted that this simulation does not consider the extracellular diffusion barrier and lipid membrane permeability.

The one-dimensional concentration changes of free NO molecules and unbound free hemes in each unit in one HbV ([Hb]$_{in}$ = 1 and 35 g/dl) are obtained by simulations, and the results are converted to a two-dimensional scheme, as shown in Fig. 4. In the case of HbV at [Hb]$_{in}$ = 1 g/dl, both dissolved free NO and unbound free hemes are already homogeneously distributed at 5 ms, indicating that NO diffuses rapidly into HbV, and the reaction proceeds quite homogeneously. On the other hand, HbV at [Hb]$_{in}$ = 35 g/dl showed heterogeneous distribution. The concentration gradients of both NO and heme change from the interior surface to the core. Even after 100 ms, the distributions are heterogeneous.

To clarify the influence of D_{NO} that changes with [Hb]$_{in}$ (Table 2), D_{NO} was fixed to the value in the bulk solution (2210 $\mu m^2\ s^{-1}$) to all HbV with different [Hb]$_{in}$. As shown in Fig. 5, the difference in $k'_{on}^{(NO)}$ is minimized considerably in comparison with the condition of variable D_{NO} at each [Hb]$_{in}$. This indicates that the lowered D_{NO} in the highly concentrated viscous Hb solution contributes considerably to the retardation of NO binding.

Extrapolation to Larger Particles (1000–8000 nm)—Computer simulations were performed to larger particles (diameter, 1000, 2000, and 8000 nm) in addition to smaller particles (≤500 nm); their apparent binding rate constants, $k'_{on}^{(NO)}$ and $k'_{on}^{(CO)}$, are plotted against the diameter to clarify the influence of diameters of particles encapsulating the 1 and 35 g/dl Hb solutions (Fig. 6). The experimental values of the Hb solution and HbV are also plotted; they show good coincidence. At [Hb]$_{in}$ = 35 g/dl, both NO binding and CO binding are remarkably retarded with larger diameters. Interestingly, there were threshold diameters for retardation of both NO and CO bindings, around 100 nm for $k'_{on}^{(NO)}$ and 1000 nm for $k'_{on}^{(CO)}$. Although HbV with smaller diameters shows almost identical $k'_{on}^{(CO)}$, the results of our computer simulation suggest that particles larger than 1000 nm would show retardation of CO binding in much the same manner as that with NO binding. At [Hb]$_{in}$ = 1 g/dl, both NO binding and CO binding showed less change in the binding rate constants that coincide the experimental results; however, the simulation predicts that the retardation becomes obvious with particles larger than ~1000 nm for NO binding, and

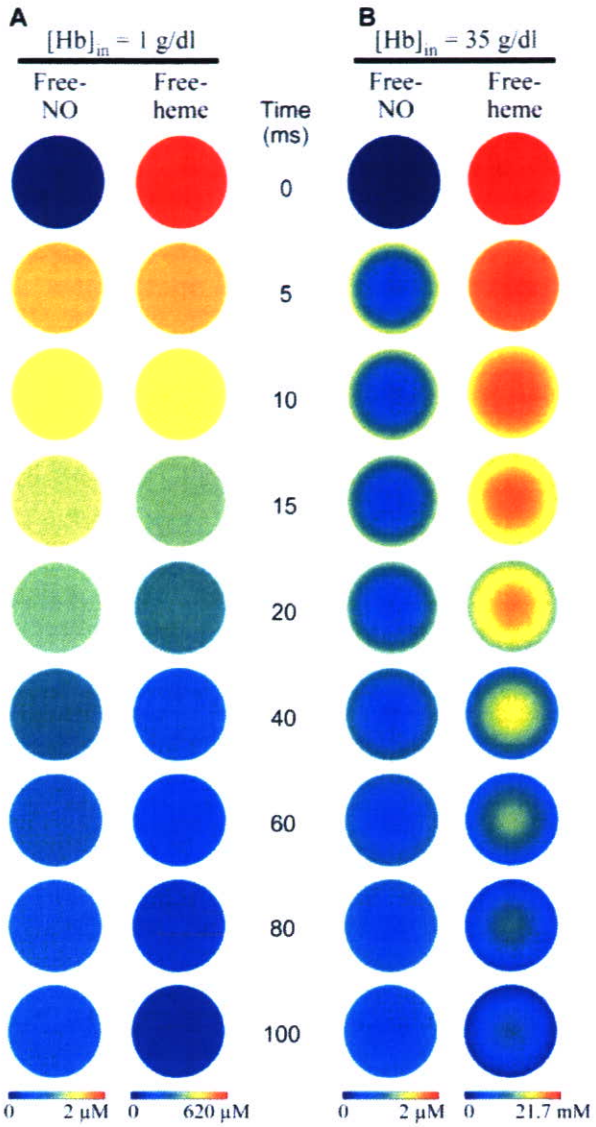

FIGURE 4. **Schematic two-dimensional representation of the simulated time courses of distributions of unbound free NO and unbound free heme in one HbV (250 nm).** *A*, at $[Hb]_{in}$ = 1 g/dl, both free NO and unbound hemes are distributed homogeneously at 5 ms, indicating that NO diffuses rapidly into HbV; the reaction proceeds homogeneously. *B*, at $[Hb]_{in}$ = 35 g/dl, both free NO and unbound hemes are distributed heterogeneously at any time. The concentration changes gradually from the surface to the core, indicating formation of the intracellular diffusion barrier. Particle diameter is fixed at 250 nm. It is easily speculated from the results that such gradients will be enhanced in larger particles.

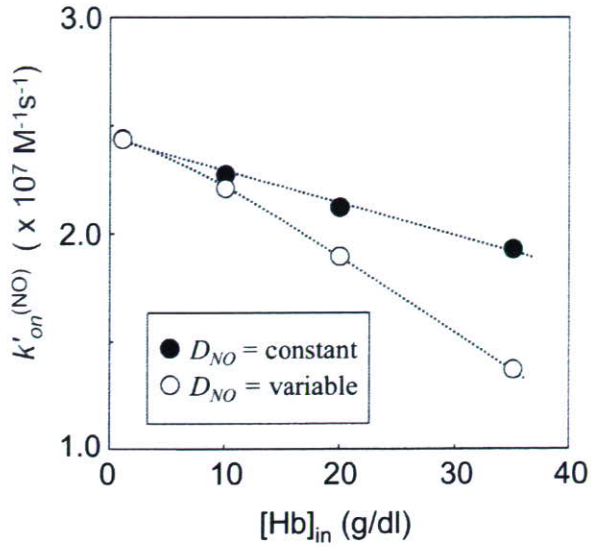

FIGURE 5. **Influence of D_{NO} on the retardation of NO binding to HbV.** Computer simulations of NO binding to HbV were performed under the assumption that the diffusion constant of NO (D_{NO}) is independent of $[Hb]_{in}$ (*closed circles*). D_{NO} was fixed to the value in the bulk solution (2210 $\mu m^2 s^{-1}$) to all HbV with different $[Hb]_{in}$. The HbV with a higher $[Hb]_{in}$ showed a slower rate of binding. However, the slope becomes gentle in comparison with the results of variable D_{NO} at each $[Hb]_{in}$ as shown in Table 2 (*open circles*). This indicates the contribution of the reduced D_{NO} in a highly viscous Hb solution to the retardation of NO binding. Particle diameter is fixed at 250 nm.

~2000 nm for CO binding. We can estimate the apparent binding rate constant of a particle encapsulating a 35-g/dl Hb solution with 8000-nm diameter, and $k'_{on}{}^{(NO)}$ and $k'_{on}{}^{(CO)}$ will be reduced to 5.6×10^5 and 7.3×10^4 $M^{-1} s^{-1}$, respectively. Overall, encapsulation of a 35-g/dl Hb solution in an 8000-nm particle would retard the NO binding by 2 orders and the CO binding by 1 order in comparison with the corresponding elementary reactions of the cell-free Hb solution.

DISCUSSION

Our primary finding is that NO binding of Hb is considerably retarded when a concentrated Hb solution is encapsulated in phospholipid vesicles (liposomes). On the other hand, CO binding of Hb shows no such retardation by encapsulation with particle size smaller than 500 nm. The phospholipid bilayer membrane itself has no barrier function to the gas diffusion, because the apparent binding rate constants of both NO and CO at $[Hb]_{in}$ = 1 g/dl and those of an acellular Hb solution were almost identical. In this study, using computer simulations, we propose that the determinant factor of retardation should be the intracellular, not extracellular, gas diffusion barrier in the case of HbV, which was induced by (i) the considerably large binding rate constant of NO to a heme of an Hb molecule, (ii) the numerous hemes as sites of gas entrapment at a high $[Hb]_{in}$, (iii) the slowed gas diffusion in the intracellular viscous Hb solution, and (iv) the longer diffusion distance in the larger particle diameter of the capsule (Fig. 7).

We reported the retardation of NO binding by Hb encapsulation in 1996 (30), which was earlier than the 1998 report of Liu *et al.* (6), who first showed that NO binding of Hb is retarded by the RBC cellular membrane. Rudolph *et al.* (26) attempted stopped-flow spectrophotometry of liposome-encapsulated Hb in 1997, expecting the retardation of the NO reaction by Hb encapsulation, but they identified no effect that was likely to have been attributable to the low $[Hb]_{in}$ (<14 g/dl) of their liposome-encapsulated Hb. In the present study, we intended more detailed analyses to clarify the mechanism of retardation, because it seems to have remained controversial in the last decade (20). It seems to us that these controversies are attributable to the complex and fragile structure of RBC and chemically unstable NO, which make it difficult to analyze the NO binding of RBC without causing hemolysis (2, 50). So-called competition experiments have been conducted between free Hb and RBC at a high hematocrit that would be a physiologically more

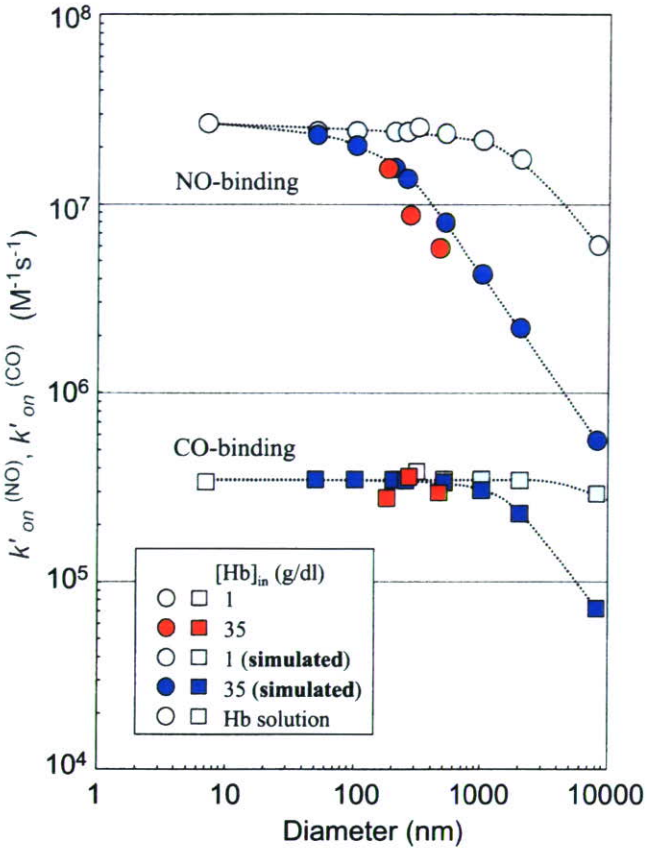

FIGURE 6. **Computer simulations of NO binding and CO binding by particles with different particle diameter.** At $[Hb]_{in}$ = 35 g/dl, the apparent CO binding rate constant, $k'_{on}{}^{(CO)}$, is almost identical up to 1000 nm in diameter; then it is reduced considerably, concomitant with increasing the diameter (*blue squares* in the *bottom*). On the other hand, $k'_{on}{}^{(NO)}$ decreases slightly up to 100 nm diameter; it then decreases steeply with enlarging particle diameter (*blue circles* in the *top*). In the case of $[Hb]_{in}$ = 1 g/dl, both NO binding (*light blue circles*) and CO binding (light blue squares) showed less change in the binding rate constants. However, the retardation becomes obvious when the particle diameter is larger than ~1000 nm for NO binding and even for CO binding when the diameter is larger than ~2000 nm. Experimental values for the Hb solution (*white circle* and *square*) and HbV (*pink* or *red squares* and *circles*) are close to the simulated values. The apparent binding rate constants, $k'_{on}{}^{(NO)}$ and $k'_{on}{}^{(CO)}$, of a spherical particle with diameter of 8000 nm and $[Hb]_{in}$ = 35 g/dl are estimated to be reduced to 5.6×10^5 and 7.3×10^4 M^{-1} s^{-1}, respectively. The reported $k'_{on}{}^{(NO)}$ values of a series of chemically modified HBOCs (diameter, 6–28 nm), about 3.0×10^7 M^{-1} s^{-1}, were identical to that of an unmodified Hb solution (38), which coincided well with our simulation.

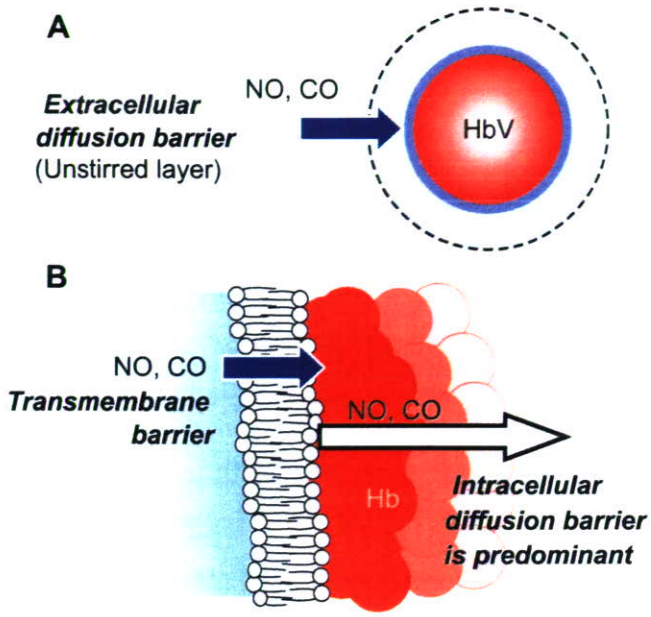

FIGURE 7. **Proposed mechanisms of retardation of gas binding by encapsulated Hbs.** *A*, it has been suggested that an unstirred layer near the outer surface of a cell would become an extracellular diffusion barrier to retard ligand bindings. However, our experimental results and computer simulations suggest that this is not a major process for retardation of ligand bindings in the case of HbV. *B*, the phospholipid bilayer membrane cannot have any barrier function to gas diffusion, because the apparent binding rate constants of both NO and CO at $[Hb]_{in}$ = 1 g/dl were close to those of an acellular Hb solution, as shown in Fig. 3. We propose that the determinant factor of retardation should be the intracellular diffusion barrier in the case of HbV, which is induced by (i) an intrinsically larger binding rate constant of NO to a heme in an Hb molecule, (ii) numerous hemes as sites of gas entrapment at a higher $[Hb]_{in}$, (iii) a slowed gas diffusion in the intracellular viscous Hb solution, and (iv) a longer gas diffusion distance in a larger capsule.

relevant condition (7, 50). However, it remains unclear for us whether the heterogeneous condition of a concentrated RBC suspension in a more static condition would be appropriate for an accurate kinetic measurement. Resealed RBCs were prepared to reduce the submembrane cytoskeletal layer or to reduce $[Hb]_{in}$ (2, 23), but it remains unknown whether hemolysis was suppressed completely after the complicated procedure and whether the electrolyte concentrations were maintained that might influence the Hb allostery and the resulting ligand binding profiles. We surmised that utilization of HbV, an artificially prepared model of RBC, would enable a systematic analysis, because the physicochemical parameters of HbV are adjustable, such as high $[Hb]_{in}$ up to 35 g/dl and particle diameter in a narrow range of P_{50}. Moreover, the physical stability of HbV is unexpectedly sufficient for stopped-flow spectrophotometry. We intentionally selected a low NO concentration (1.9 μM) to monitor the whole reaction of NO binding. Precedent reports of stopped-flow spectrophotometry of RBC at a higher NO concentration presented the problem not only of hemolysis but also the rate of NO reaction. It is so fast that a substantial part of the process occurs during the dead time (1–2 ms). On the other hand, in our study, a pseudo-first-order reaction is not appropriate for NO binding, and we calculated $k'_{on}{}^{(NO)}$ from the initial phase of the reaction because of a low NO concentration compared with the heme concentration. In such a condition, some redox charge transfer reaction would occur between heme and NO at a lower NO concentration (51). Another limitation of our simulation is the wide size distribution of HbV prepared using the extrusion method. $[Hb]_{in}$ was the concentration of the fed Hb solution for encapsulation, and we did not directly measure $[Hb]_{in}$ after encapsulation. These would be reasons for the deviation of the experimental results and the simplified computer simulation. However, it should be noted that our computer simulations recreated the tendencies of the experimental results of the ligand binding profiles of HbV.

In the computer simulation, we did not include the extracellular diffusion barrier, because HbV (250 nm) is much smaller than RBC (8 μm), and the diffusion of HbV as a particle should be much faster than that of RBC according to the Stokes-Einstein equation. The extracellular fluid near the surface should be stirred by the rapid movement of HbV. It is expected that the

thickness of the unstirred layer as an extracellular diffusion barrier would be much less for small HbV than that for RBC (1–3 μm) (2). Actually, results of the present computer simulations of HbV without consideration of the extracellular diffusion barrier clarified that the intracellular diffusion resistance is sufficient to explain the retardation of NO binding in the results of stopped-flow spectrophotometry, and possibly, our findings might suggest that the extracellular diffusion barrier is negligible even for RBC. This supports the results of Vaughn *et al.* (7) that the extracellular diffusion resistance is negligible. However, our data do not directly support the presence of transmembrane diffusion limitation, because the HbV at $[Hb]_{in}$ = 1 g/dl and the cell-free Hb solution showed nearly identical $k'_{on}{}^{(NO)}$; actually, the computer simulation did not require the consideration of the membrane barrier. Han *et al.* (23) proposed that a submembrane cytoskeletal barrier would induce the resistance to the NO binding to bovine RBC using the RBC ghost. This might be possible to some extent if the submembrane cytoskeleton were to contain densely layered heme proteins such as adsorbed Hbs that could be the sites of rapidly binding NO. However, we believe that the intracellular concentrated Hb solution (about 35 g/dl) near the cytoskeleton of RBC can be the predominant barrier to further NO diffusion into RBC. Liu *et al.* (19) described that "NO that enters into RBC is immediately scavenged by the concentrated intracellular Hb so that NO concentration inside the RBC is maintained very close to zero," although they did not pay attention to it as the intracellular diffusion barrier.

The binding rate constant of CO of cell-free Hb molecule ($k_{on}{}^{(CO)}$) is well known to be much smaller than those of NO and O_2 (52). The rate-limiting step for CO binding is the internal bond formation with the heme iron. In fact, based on the electron theory, CO enters the globin hundreds of times before it finally forms a bond with the iron atom. Consequently, the overall bimolecular rate constant is normally small (53). The experimental finding that CO binding shows negligible retardation, even after encapsulation in HbV, also supports our proposal that rapid NO binding causes the sink of NO at the interior surface region of HbV and retards further NO diffusion into the core of HbV in combination of the lowered D_{NO} in the highly concentrated viscous Hb solution (45–48). However, it is expected that HbV with a much larger diameter can contribute to retardation, even for CO binding, as clarified by our computer simulation. Coin and Olson (2) compared the bindings of O_2, CO, and ethyl isocyanate to Hb with their elementary reaction constants, k_{on}, of 3×10^6, 2.0×10^5, and 2.1×10^4 M^{-1} s^{-1}, respectively (1:10 and 1:100 differences). Results of that study showed that the difference between k_{on} of Hb and k'_{on} of RBC decreases for a slower reaction. The difference becomes very small for the binding of ethyl isocyanate, which clearly supports our data; a faster reaction tends to induce a stronger intracellular diffusion barrier and retards the reaction in comparison with the cell-free Hb solution.

In blood circulation in the presence of O_2, NO is inactivated mainly by NO dioxygenation by O_2-bound HBOCs and RBC. According to Herold *et al.* (54), the rate constant of the elementary reaction, HbO_2 and NO, is 8.9×10^7 M^{-1} s^{-1}, which is faster than that of deoxyHb (2.6×10^7 M^{-1} s^{-1}). We predict that the reaction with HbO_2 should be much faster to form an intracellular diffusion barrier than that with deoxyHb. Consequently, the contribution of Hb encapsulation to the retardation should be pronounced. This can support the results of Azarov *et al.* (50) and Huang *et al.* (21), which showed that "the membrane barrier function" becomes more effective in limiting NO uptake for oxygenated RBC than the deoxygenated RBC, although their proposing mechanism is different from ours.

Our computer simulation system would be an effective tool to predict the ligand binding profiles of HbV with different Hb concentration and different particle size and other imaginary parameters. This can roughly simulate the NO binding and CO binding profiles of a spherical particle with a diameter identical to that of the major axis of RBC. The values of $k'_{on}{}^{(NO)}$ and $k'_{on}{}^{(CO)}$ of a spherical particle encapsulating 35-g/dl Hb with a diameter of about 8 μm are estimated, respectively, as 5.6×10^5 and 7.3×10^4 M^{-1} s^{-1}. Those values resemble the precedent values of human RBC measured using stopped-flow spectrophotometry without causing hemolysis (<5%): $k'_{on}{}^{(NO)}$, 1.2×10^5 M^{-1} s^{-1}; $k'_{on}{}^{(CO)}$, 6.5×10^4 M^{-1} s^{-1} (55); and $k'_{on}{}^{(CO)}$, 6.0×10^4 M^{-1} s^{-1} (31). On the other hand, our simulated $k'_{on}{}^{(NO)}$ would be faster than the values of RBC; 5.2×10^4 M^{-1} s^{-1} (6) and 1.4×10^4 M^{-1} s^{-1} (50), which are contradictorily much smaller than the CO binding rate constants of the above, which might suggest the presence of other mechanisms, such as the unstirred layer as the extracellular diffusion barrier in the case of large RBCs that diffuse slowly at a high Hct in their experiments. Even so, the retardation seems to be mainly induced by the intracellular diffusion barrier, because $k'_{on}{}^{(NO)}$ is reduced by 2 orders of magnitude in comparison with a cell-free Hb. Alternatively, we might consider the biconcave disk structure of RBC. Different P_{50} values of HbV (13–16 torrs) in comparison with that of human RBC (28 torrs) might also influence the binding rates.

Interestingly, the presence of the threshold diameters for retardation of ligand bindings is apparent, as shown in Fig. 6. The threshold diameter for CO is larger than that for NO, indicating that the slower reaction of CO binding allows a longer distance of gas diffusion before induction of an intracellular diffusion barrier than it allows with the more rapid NO binding. The rate-determining steps are the elementary gas-binding reaction for particles smaller than the threshold diameter and the gas diffusion for larger particles. It should be noted that the retardation is predicted for the larger particles at $[Hb]_{in}$ = 1 g/dl, although the threshold diameter is increased to 1000 nm for NO binding and 2000 nm for CO binding.

The retardation of NO binding by Hb encapsulation cannot fully explain the phenomenon that HbV with a diameter of ~250 nm does not induce vasoconstriction after intravenous injection (13), because $k'_{on}{}^{(NO)}$ of HbV is much larger than that of RBC (10^4 to 10^5 M^{-1} s^{-1}). Any HBOC is much smaller in size than RBC and is distributed homogeneously in the plasma layer (5). Therefore, an RBC-free zone at the blood/endothelium interface becomes an HBOC-dissolved zone and might be a sink of NO (56, 57). Rohlfs *et al.* (38) reported that the NO binding rate constants of a series of chemically modified HBOCs (diameter, 6–28 nm) (58), measured using the laser flash photolysis, were identical to that of an unmodified Hb

solution, about 3.0×10^7 M^{-1} s^{-1}, which coincided well with our simulation in Fig. 6; particles with a diameter of less than 50 nm are almost identical. They concluded straightforwardly that NO uptake was not related to vasoconstriction, because polyethylene glycol-modified Hb did not exceptionally induce vasoconstriction, and other mechanisms are actually suggested in relation to molecular recognition and oxygen affinity (11, 59). We speculate the presence of another threshold particle diameter to penetrate across the perforated endothelial cell layer to approach a space (such as the space of Disse near the sinusoidal endothelial layer in a hepatic microcirculation or the space between the endothelium and the smooth muscle) where CO or NO is produced as a vasorelaxation factor to bind to soluble guanylate cyclase, which catalyzes the conversion of guanosine triphosphate to cyclic guanosine monophosphate (13, 18, 60, 61). As summarized by Olson *et al.* (16), both the retardation of the NO reaction (reduced NO affinity) (62) and the larger particle diameter are inferred to be keys to suppress vasoconstriction and hypertension induced by HBOCs.

In summary, we suggest the significant contribution of the intracellular diffusion barrier and the absence of lipid membrane barrier for NO uptake in the case of HbV. We speculate that the same findings might apply to RBCs. Although some discrepancies exist between the experimental results and computer simulations, we are surprised that such a simple simulation system can be an effective tool to predict the ligand binding reaction of HbV and larger particles, although the system is based merely on physicochemical parameters: the gas diffusion constant and elementary reaction rate constants. Our data provide a new insight into the cellular structures of RBC and HbV as an artificial oxygen carrier. Our next step will be to apply this system to recreate the ligand binding profiles of a biconcave disk shaped or parachute-like RBC and HbV suspension flowing heterogeneously in microvessels and in an artificial gas-permeable narrow tube (5) to identify additional mechanisms of the absence of vasoconstriction.

Acknowledgments—We thank Prof. M. Intaglietta (University of California, San Diego) and Prof. M. Suematsu (Keio University) for discussion related to the mechanism of ligand binding.

REFERENCES

1. Hartridge, H., and Roughton, F. J. W. (1927) *J. Physiol.* **62,** 232–242
2. Coin, J. T., and Olson, J. S. (1979) *J. Biol. Chem.* **254,** 1178–1190
3. Vandegriff, K. D., and Olson, J. S. (1984) *J. Biol. Chem.* **259,** 12619–12627
4. Page, T. C., Light, W. R., McKay, C. B., and Hellums, J. D. (1998) *Microvasc. Res.* **55,** 54–66
5. Sakai, H., Suzuki, Y., Kinoshita, M., Takeoka, S., Maeda, N., and Tsuchdia, E. (2003) *Am. J. Physiol.* **285,** H2543–H2555
6. Liu, X., Miller, M. J., Joshi, M. S., Sadowska-Krowicka, H., Clark, D. A., and Lancaster, J. R., Jr. (1998) *J. Biol. Chem.* **273,** 18709–19713
7. Vaughn, M. W., Huang, K. T., Kuo, L., and Liao, J. C. (2000) *J. Biol. Chem.* **275,** 2342–2348
8. Minneci, P. C., Deans, K. J., Zhi, H., Yuen, P. S., Star, R. A., Banks, S. M., Schechter, A. N., Natanson, C., Gladwin, M. T., and Solomon, S. B. (2005) *J. Clin. Invest.* **115,** 3409–3417
9. Hess, J. R., MacDonald, V. W., and Brinkley, W. W. (1993) *J. Appl. Physiol.* **74,** 1769–1778
10. Sloan, E. P., Koenigsberg, M., Gens, D., Cipolle, M., Runge, J., Mallory, M. N., and Rodman, G., Jr. (1999) *J. Am. Med. Assoc.* **282,** 1857–1864
11. Gulati, A., Barve, A., and Sen, A. P. (1999) *J. Lab. Clin. Med.* **133,** 112–119
12. Rochon, G., Caron, A., Toussaint-Hacquard, M., Alayash, A. I., Gentils, M., Labrude, P., Stoltz, J. F., and Menu, P. (2004) *Hypertension* **43,** 1110–1115
13. Sakai, H., Hara, H., Yuasa, M., Tsai, A. G., Takeoka, S., Tsuchida, E., and Intaglietta, M. (2000) *Am. J. Physiol.* **279,** H908–H915
14. Nakai, K., Ohta, T., Sakuma, I., Akama, K., Kobayashi, Y., Tokuyama, S., Kitabatake, A., Nakazato, Y., Takahashi, T. A., and Sekiguchi, S. (1996) *J. Cardiovasc. Pharmacol.* **28,** 115–123
15. Bunn, H. F. (1995) *Transfus. Clin. Biol.* **2,** 433–439
16. Olson, J. S., Foley, E. W., Rogge, C., Tsai, A. L., Doyle, M. P., and Lemon, D. D. (2004) *Free Radic. Biol. Med.* **36,** 685–697
17. Suematsu, M., Goda, N., Sano, T., Kashiwagi, S., Egawa, T., Shinoda, Y., and Ishimura, Y. (1995) *J. Clin. Invest.* **96,** 2431–2437
18. Goda, N., Suzuki, K., Naito, M., Takeoka, S., Tsuchida, E., Ishimura, Y., Tamatani, T., and Suematsu, M. (1998) *J. Clin. Invest.* **101,** 604–612
19. Liu, X., Samouilov, A., Lancaster, J. R., Jr., and Zweier, J. L. (2002) *J. Biol. Chem.* **277,** 26194–26199
20. Kim-Shapiro, D. B., Schechter, A. N., and Gladwin, M. T. (2006) *Arterioscler. Thromb. Vasc. Biol.* **26,** 697–705
21. Huang, K. T., Huang, Z., and Kim-Shapiro, D. B. (2007) *Nitric Oxide* **16,** 209–216
22. Huang, K. T., Han, T. H., Hyduke, D. R., Vaughn, M. W., Van Herle, H., Hein, T. W., Zhang, C., Kuo, L., and Liao, J. C. (2001) *Proc. Natl. Acad. Sci. U. S. A.* **98,** 11771–11776
23. Han, T. H., Pelling, A., Jeon, T. J., Gimzewski, J. K., and Liao, J. C. (2005) *Biochim. Biophys. Acta* **1723,** 135–142
24. Sakai, H., Masada, Y., Horinouchi, H., Yamamoto, M., Ikeda, E., Takeoka, S., Kobayashi, K., and Tsuchida, E. (2004) *Crit. Care Med.* **32,** 539–545
25. Sakai, H., Horinouchi, H., Yamamoto, M., Ikeda, E., Takeoka, S., Takaori, M., Tsuchida, E., and Kobayashi, K. (2006) *Transfusion* **46,** 339–347
26. Rudolph, A. S., Sulpizio, A., Hieble, P., MacDonald, V., Chavez, M., and Feuerstein, G. (1997) *J. Appl. Physiol.* **82,** 1826–1835
27. Chang, T. M. (2006) *Artif. Cells Blood Substit. Biotechnol.* **34,** 551–566
28. Djordjevich, L., and Miller, I. F. (1982) *Exp. Hematol.* **8,** 584–592
29. Sakai, H., Tomiyama, K. I., Sou, K., Takeoka, S., and Tsuchida, E. (2000) *Bioconjugate Chem.* **11,** 425–432
30. Sakai, H., Hamada, K., Takeoka, S., Nishide, H., and Tsuchida, E. (1996) *Polymer Adv. Technol.* **7,** 639–644
31. Olson, J. S. (1981) *Methods Enzymol.* **76,** 631–651
32. Takeoka, S., Ohgushi, T., Terase, K., Ohmori, T., and Tsuchida, E. (1996) *Langmuir* **12,** 1755–1759
33. Sakai, H., Tsai, A. G., Rohlfs, R. J., Hara, H., Takeoka, S., Tsuchida, E., and Intaglietta, M. (1999) *Am. J. Physiol.* **276,** H553–H562
34. Takeoka, S., Terase, K., Yokohama, H., Sakai, H., Nishide, H., and Tsuchida, E. (1994) *J. Macromol. Sci. Pure Appl. Chem., Part A* **31,** 97–108
35. Wang, L., Morizawa, K., Tokuyama, S., Satoh, T., and Tsuchida, E. (1992) *Polymer Adv. Technol.* **4,** 8–11
36. Sakai, H., Takeoka, S., Yokohama, H., Seino, Y., Nishide, H., and Tsuchida, E. (1993) *Protein Expression Purif.* **4,** 563–569
37. Sakai, H., Masada, Y., Takeoka, S., and Tsuchida, E. (2002) *J. Biochem. (Tokyo)* **131,** 611–617
38. Rohlfs, R. J., Bruner, E., Chiu, A., Gonzales, A., Gonzales, M. L., Magde, D., Magde, M. D. Jr., Vandegriff, K. D., and Winslow, R. M. (1998) *J. Biol. Chem.* **273,** 12128–12134
39. Szebeni, J., Breuer, J. H., Szelenyi, J. G., Bathori, G., Lelkes, G., and Hollan, S. R. (1984) *Biochim. Biophys. Acta* **798,** 60–67
40. Szebeni, J., Di Iorio, E. E., Hauser, H., and Winterhalter, K. H. (1985) *Biochemistry* **24,** 2827–2832
41. Baker, P. R., Lin, Y., Schopfer, F. J., Woodcock, S. R., Groeger, A. L., Batthyany, C., Sweeney, S., Long, M. H., Iles, K. E., Baker, L. M., Branchaud, B. P., Chen, Y. E., and Freeman, B. A. (2005) *J. Biol. Chem.* **280,** 42464–42475
42. Yokohama, H., Seino, Y., Chung, J., Sakai, H., Takeoka, S., Nishide, H., and Tsuchida, E. (1994) *Artif. Organs Today* **4,** 107–116
43. Sou, K., Naito, Y., Endo, T., Takeoka, S., and Tsuchida, E. (2003) *Biotechnol. Prog.* **19,** 1547–1552
44. Sakai, H., Hamada, K., Takeoka, S., Nishide, H., and Tsuchida, E. (1996) *Biotechnol. Prog.* **12,** 119–125
45. Nishide, H., Chen, X., and Tsuchida, E. (1997) *Artif. Cells Blood Substit.*

Immobil. Biotechnol. **25,** 335–346
46. Chen, X., Nishide, H., and Tsuchida, E. (1996) *Bull Chem. Soc. Jpn.* **69,** 255–259
47. Bouwer, S. T., Hoofd, L., and Kreuzer, F. (1997) *Biochim. Biophys. Acta* **1338,** 127–136
48. Minton, A. P., and Ross, P. D. (1978) *J. Phys. Chem.* **82,** 1934–1938
49. Sakai, H., Tomiyama, K., Masada, Y., Takeoka, S., Horinouchi, H., Kobayashi, K., and Tsuchida, E. (2003) *Clin. Chem. Lab. Med.* **41,** 222–231
50. Azarov, I., Huang, K. T., Basu, S., Gladwin, M. T., Hogg, N., and Kim-Shapiro, D. B. (2005) *J. Biol. Chem.* **280,** 39024–39032
51. Gow, A. J., and Stamler, J. S. (1998) *Nature* **391,** 169–173
52. Rose, E. J., and Hoffman, B. M. (1983) *J. Am. Chem. Soc.* **105,** 2866–2873
53. Olson, J. S., Foley, E. W., Maillett, D. H., and Paster, E. V. (2003) *Methods Mol. Med.* **82,** 65–91
54. Herold, S., Exner, M., and Nauser, T. (2001) *Biochemistry* **40,** 3385–3395
55. Carlsen, E., and Comroe, J. H. (1958) *J. Gen. Physiol.* **42,** 83–107
56. Kavdia, M., Tsoukias, N. M., and Popel, A. S. (2002) *Am. J. Physiol.* **282,** H2245–H2253
57. Jeffers, A., Gladwin, M. T., and Kim-Shapiro, D. B. (2006) *Free Radic. Biol. Med.* **41,** 1557–1565
58. Vandegriff, K. D., McCarthy, M., Rohlfs, R. J., and Winslow, R. M. (1997) *Biophys. Chem.* **69,** 23–30
59. Tsai, A. G., Cabrales, P., Manjula, B. N., Acharya, S. A., Winslow, R. M., and Intaglietta, M. (2006) *Blood* **108,** 3603–3610
60. Nakai, K., Sakuma, I., Ohta, T., Ando, J., Kitabatake, A., Nakazato, Y., and Takahashi, T. A. (1998) *J. Lab. Clin. Med.* **132,** 313–319
61. Matheson, B., Kwansa, H. E., Bucci, E., Rebel, A., and Koehler, R. C. (2002) *J. Appl. Physiol.* **93,** 1479–1486
62. Doherty, D. H., Doyle, M. P., Curry, S. R., Vali, R. J., Fattor, T. J., Olson, J. S., and Lemon, D. D. (1998) *Nat. Biotechnol.* **16,** 672–676

ARTICLE IN PRESS

BBAMEM-79633; No. of pages: 7; 4C: 2, 4, 5

Available online at www.sciencedirect.com

ScienceDirect

Biochimica et Biophysica Acta xx (2008) xxx–xxx

Biochimica et Biophysica Acta BBA

www.elsevier.com/locate/bbamem

Electrostatic interactions and complement activation on the surface of phospholipid vesicle containing acidic lipids: Effect of the structure of acidic groups

Keitaro Sou, Eishun Tsuchida *

Research Institute for Science and Engineering, Waseda University, Tokyo 169-8555, Japan

Received 5 September 2007; received in revised form 22 November 2007; accepted 7 January 2008

Abstract

Anionic vesicles containing acidic phospholipids are known complement activators. To clarify which negative physicochemical electrostatic charges on vesicles and structural specificities of acidic lipids are critical to complement activation, the electrostatic properties and activity to complement of two anionic vesicles modified with a carboxylic acid derivative or a conventional acidic phospholipid were compared. Electrophoretic mobility measurements indicated that the negative zeta potential and the electrostatic interactivity of these two anionic vesicles were equal at pH 7.4. However, the infusion of vesicles containing acidic phospholipid induced significant complement activation, while vesicles containing the carboxylic acid derivative failed to activate complement. These results indicate that the negative charge on the surface of vesicles is not critical for the activation complement, suggesting that complement activation is specific to the structure of acidic groups. This finding is likely to be important to the design of anionic biointerfaces and may support the promising medical applications of this anionic vesicle modified with a carboxylic acid derivative.

Keywords: Liposome; Acidic lipid; Anionic surface; Electrostatic interaction; Complement activation

1. Introduction

Anionic vesicles (liposomes), commonly formulated by mixing acidic phospholipids such as phosphoglycerol, phosphoserin, phosphoinositol, phosphatidic acid, cardiolipin, and poly (ethylene glycol) (PEG) conjugated phosphoethanolamine in lipid components are known to mediate complement activation [1–5]. Complement activation, which is followed by systemic immune activation and anaphylaxis shock, is regarded as a critical problem in the clinical setting of various biomaterials. The C1q subcomponent of C1 has a highly cationic region in residues 14–26 of the C1qA polypeptide chain, and this specific region of the collagenous stalk of C1q has been identified as being involved in interactions with negatively charged activators [5–8]. It is believed that the antibody-independent binding of C1q to the negatively charged surface of vesicles initiates the activation of the complement cascade via the classical complement pathway [2]. To prevent complement activation, the acidic phospholipids can be removed or their negative charge can be protected by chemical modification [2,4]. It has also been reported that surface modification with a dense PEG layer is effective for preventing complement activation by covering the surface charge [9].

Our group has developed phospholipid vesicles called hemoglobin-vesicles that encapsulate human hemoglobin and that can be used as a substitute for red blood cells and as an alternative to conventional transfusion [10–14]. To achieve this challenging application of vesicles, we had to develop anionic vesicles capable of encapsulating hemoglobin using a minimum amount of lipids, retaining the negative charge on the membrane which reduces the lamellarity of vesicles and is required for improving encapsulation capacity [11–13]. Several acidic lipids have been tested and a carboxylic acid derivative, L-glutamic

* Corresponding author. Tel.: +81 3 5286 3120; fax: +81 3 3205 4740.
E-mail addresses: ksou@waseda.jp (K. Sou), eishun@waseda.jp (E. Tsuchida).

0005-2736/$ - see front matter © 2008 Elsevier B.V. All rights reserved.
doi:10.1016/j.bbamem.2008.01.006

acid, *N*-(3-carboxy-1-oxopropyl)-, 1,5-dihexadecyl ester (SA), has been used as an anionic component. Vesicles containing SA have been demonstrated to efficiently encapsulated hemoglobin, and given their stability, can be infused in considerably large doses as a red blood cell substitute [15,16]. In addition, administration of this formulation is not associated with considerable rejection by the blood immune system and complement in animals [17,18]. Recent collaboration involving our group found that vesicles containing SA are selectively captured by bone marrow macrophages at small injection doses in rabbits [19]. This targeting of bone marrow has not yet been reported for conventional anionic vesicles. These findings suggest that the surface characteristics of the anionic vesicles have a marked effect on their associated biological events and that this is highly dependent upon the nature of the acidic groups.

Based on the hypothesis that the negative electrostatic charge of acidic phospholipids on the surface of vesicles is one of the factors responsible for inducing complement activation, the electrostatics of vesicles containing SA may differ from those of vesicles containing acidic phospholipids. Conversely, when the electrostatic interactivity of these acidic lipids is equal, biological events such as complement activation are likely to be mediated by the molecular specificity of acidic lipids. To elucidate what aspects are critical to the biocompatibility and performance of anionic vesicles, a comparative analysis of the electrostatic interfacial properties of vesicles containing either SA or acidic phospholipids is essential. In this study, we elucidated the electrostatic interfacial properties of vesicles containing SA or an acidic phospholipid by electrophoretic mobility measurement and observed complement activation after the infusion of these vesicles in animals. The results clearly demonstrated that the negatively charged group on the surface of anionic vesicles is not critical to the activation of complement.

2. Materials and methods

2.1. Materials

1,2-Dipalmitoyl-*sn*-glycero-3-phosphocholine (PC), cholesterol (CH), and 1,2-dipalmitoyl-*sn*-glycero-3-phosphoglycerol (PG), and L-glutamic acid, *N*-(3-carboxy-1-oxopropyl)-, 1,5-dihexadecyl ester (SA), were purchased from Nippon Fine Chemical Co. Ltd. (Osaka, Japan). 1,2-Distearoyl-*sn*-glycero-3-phosphoethanolamine-*N*-[monomethoxy poly(ethylene glycol) (5000)] (PEG-DSPE) was purchased from NOF Co. (Tokyo, Japan). Pentalysine and poly-L-lysine (Mw. 15–30 kDa) were purchased from SIGMA (St. Louis, MO).

2.2. Preparation of vesicles

Vesicle samples were produced using PC and CH (1/1, m/m, PC-vesicles), and varying amounts of SA (SA-vesicles) or PG (PG-vesicles). The mixed lipids were added to 10 mM phosphate buffer (NaCl; 20 mM, pH 7.4) and the dispersion was introduced into an extruder (Lipex Biomembrane, Canada) and extruded through the membrane filters (final pore size: 0.2 μm, Isopore®, Millipore, Tokyo, Japan) under pressure using nitrogen gas. For animal experiments, vesicles were composed of PC, CH, and SA or PG (1:1:0.2 molar ratio), with 0.3 mol% of PEG-DSPE incorporated to prevent the aggregation of vesicles [20]. Samples for animal experiments were prepared under sterile conditions.

2.3. Characterization of vesicles

The diameters of the resulting vesicles were determined with a COULTER submicron particle analyzer (N4SD, Coulter, Hialeah, FL), and the average diameter ± standard deviation (SD) was calculated. The phospholipid concentration was determined using a cholineoxidase method (Phospholipid C Test Wako; Wako Pure Chem., Tokyo). Endotoxin contamination in the samples prepared for the animal experiment was determined to be less than 0.1 EU/mL by the Limulus assay test [21].

2.4. Determination of zeta potential

A 10 μL aliquot of vesicles (lipid concentration: 2 g/dL) was diluted in 2 mL of 10 mM phosphate buffer (pH 3–9, 37 °C) containing 20 mM NaCl and incubated for 1 h at 37 °C. The pH was determined using a pH meter with a pH electrode (F-52, HORIBA, Kyoto, Japan) at 37 °C and the electrophoretic mobility of vesicles (lipid concentration: 0.01 g/dL) were determined by Laser Doppler Velocimetry (Zeta-Sizer Nano ZS, Malvern Instruments, Malvern, Worcestershire, UK). Measurement conditions and parameters were as follows: 37 °C, dielectric constant 74.4 (for dilute water solution), viscosity 0.6864 cP (for dilute water solution), and the applied voltage was 20 V/cm. The zeta potential was determined by measuring the electrophoretic mobility (U_E), and the zeta potential (ζ) and applied to the Henry equation:

$$U_E = \frac{2\varepsilon\zeta f(\kappa R)}{3\eta} \quad (1)$$

where ε is the dielectric constant, η is the viscosity of the solvent, $f(\kappa R)$ is the Henry function, κ is the Debye–Hückel parameter and the R is the radius of the particle. The Smoluchowski equation was used with $f(\kappa R) = 1.5$ employed in the zeta potential calculations. Measurements were performed four times for each sample and statistical analysis was conducted using the average ± SD of the four measurements.

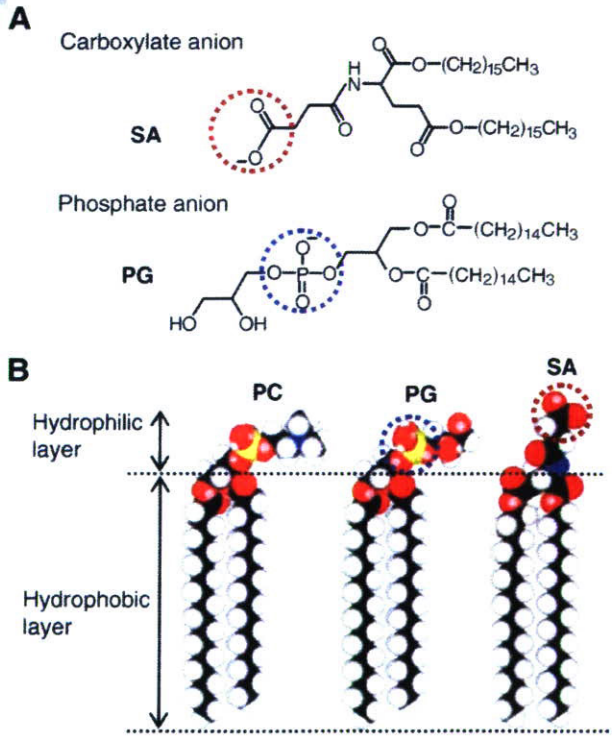

Fig. 1. Structure of anionic compounds for surface modification of vesicles. (A) Chemical structure of L-glutamic acid, *N*-(3-carboxy-1-oxopropyl)-, 1,5-dihexadecyl ester (SA) and 1,2-dipalmitoyl-*sn*-glycero-3-phosphoglycerol (PG). The focus of this study is the different acidic groups shown in the dotted circle. (B) The CPK model of SA and PG with 1,2-dipalmitoyl-*sn*-glycero-3-phosphocholine (PC) to estimate the distance of acidic groups from the membrane surface of PC. CPK models show the structure with minimized energy in molecular mechanistic calculation.

Please cite this article as: K. Sou, E. Tsuchida, Electrostatic interactions and complement activation on the surface of phospholipid vesicle containing acidic lipids: Effect of the structure of acidic groups, Biochim. Biophys. Acta (2008), doi:10.1016/j.bbamem.2008.01.006

2.5. Electrostatic interactivity

The electrostatic interactivity of the anionic vesicles was evaluated using the change in the zeta potential in presence of Ca^{2+}, pentalysine, and poly-L-lysine (Mw. 15–30 kDa) as an index. A 10 μL aliquot of vesicles (lipid concentration: 2 g/dL) was diluted in 2 mL of 10 mM 2-[4-(2-Hydroxyethyl)-1-piperazinyl] ethanesulfonic acid (HEPES) buffer (pH 7.4, 37 °C) containing 0–3 mM $CaCl_2$ and 17–20 mM NaCl (total 20 mM), or containing varying amounts of pentalysine or poly-L-lysine (Mw. 15–30 kDa) with 20 mM NaCl. The dispersions were incubated for 1 h at 37 °C before mobility measurement of the vesicles was performed by electrophoresis as described in Section 2.4.

2.6. Animal experiments

Animal experiments were conducted under the guidelines recommended by the National Institutes of Health, Animal Use and Care and the protocol was approved by the Steering Committee for Animal Experimentation at Waseda University. Male Wistar rats (250±20 g) were anesthetized with ether. The vesicular dispersion (5 g/dL) was introduced into rats through the tail veins at 1 mL/min (n=5 for each sample). Each rat received 5.6 mL/kg of body weight of vesicle dispersion (lipids: 280 mg/kg of body weight). At 1 or 24 h after injection, the blood was collected and centrifuged to separate the serum (1×10^3 g, 10 min). The collected serum was further ultracentrifuged to remove the vesicles (3×10^5 g, 30 min). The 50% hemolytic unit of complement serum (CH50) was determined in accordance with general procedures for clinical laboratory tests by a commercial company (BML, Japan).

2.7. Statistical methods

The data from the animal experiments are reported as means±standard error of the mean. Statistical analysis was performed using Microsoft Excel for Windows and CH50 values were compared using Student's unpaired t test.

3. Results and discussion

3.1. Samples

Two characteristic acidic lipids used in this study are shown in Fig. 1. SA and PG each have carboxylic acid and phosphoric acid as ionized groups, respectively. Both lipids have a strongly hydrophobic dialkyl structure to fix the ionized groups on vesicle surface. The molecular length indicated by the CPK model showed that the carboxylate anion of SA and the phosphate anion of PG would be located at the surface of PC-vesicles (Fig. 1B). Various amounts of SA and PG were incorporated into the PC/CH membrane (1:1, molar ratio) of the anionic vesicles. The size of vesicles was controlled by extrusion methods (final pore size: 0.2 μm), with final mean diameters of approximately 200 nm (Table 1). The vesicles prepared without acidic lipids

t1.1 Table 1
t1.2 Diameter of prepared vesicles containing various amounts of acidic lipid

t1.3 Acidic lipid (mol%)	Mean diameter±SD (nm)	
t1.4	SA-vesicles	PG-vesicles
t1.5 0 (PC-vesicles)	232±60	232±60
t1.6 1	224±58	230±60
t1.7 5	193±50	196±58
t1.8 9	205±40	204±49
t1.9 15	194±45	199±55
t1.10 20	198±52	194±64

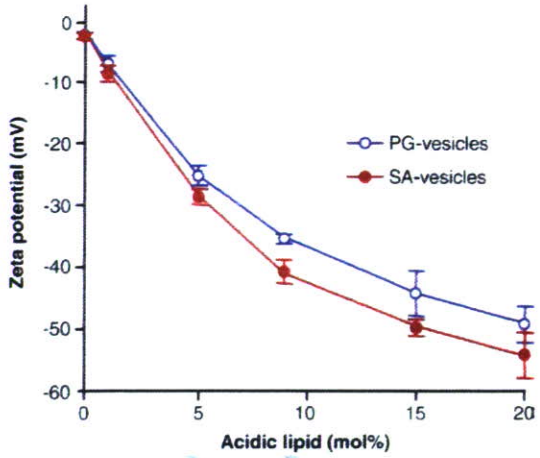

Fig. 2. Zeta potential of vesicles modified with SA (SA-vesicles) and PG (PG-vesicles) as a function of acidic lipid content. Zeta potentials were measured in 10 mM phosphate buffer (pH 7.4, NaCl; 20 mM) at 37 °C.

or with 1 mol% of acidic lipids tended to be slightly larger (ca 30 nm) than vesicles containing more acidic lipids. This effect of acidic lipids on the size of vesicles could be due to the improved dispersion stability of vesicles and electrostatic repulsion of the anionic surfaces. The vesicles without acidic lipids were observed to precipitate in a day, indicating poor dispersion stability. When the vesicles without acidic lipids contain a small amount of PEG-DSPE to prevent the aggregation of vesicles, the diameter of vesicles without acidic lipids was 202±49 nm. Therefore, we guess that the slightly large diameter of vesicles without acidic lipids or with 1 mol% of acidic lipids would be caused by the high aggregability of vesicles. The low aggregability of vesicles having a large zeta potential due to the electrostatic repulsive interaction between vesicles is an advantage of anionic vesicles as stable dispersions.

3.2. Zeta potential of vesicles

The zeta potential is the electrostatic potential at the hydrodynamic slip plane, and is characterized as having an electrical double-layer consisting of the Stern layer and the diffuse layer. Fig. 2 shows the zeta potential of prepared vesicles as a function of acidic lipid content at pH 7.4. Vesicles containing PC/CH (1:1, molar ratio) have an almost neutral surface (zeta potential: −2.22±0.62 mV), indicating that the surface is inactive for electrostatic events. The magnitude of the negative charge on the surface increased with the incorporation of SA or PG, indicating that the ionized groups of SA and PG act to characterize the vesicle surface depending on their content. The zeta potentials of SA-vesicles and PG-vesicles reached −54.2±3.68 mV and −49.0±2.89 mV for acidic lipids of 20 mol%, respectively, with the negative zeta potential of SA-vesicles being relatively higher compared to that of PG-vesicles at any concentration. In theory, the electrostatic potential is dependent upon distance from the membrane surface as well as surface charge density [22]. The slightly extended negative charge of SA from the surface shown in Fig. 1B, would reduce the distance between the change to slip plane, resulting in the higher negative zeta potential of SA-vesicles.

Please cite this article as: K. Sou, E. Tsuchida, Electrostatic interactions and complement activation on the surface of phospholipid vesicle containing acidic lipids: Effect of the structure of acidic groups, Biochim. Biophys. Acta (2008), doi:10.1016/j.bbamem.2008.01.006

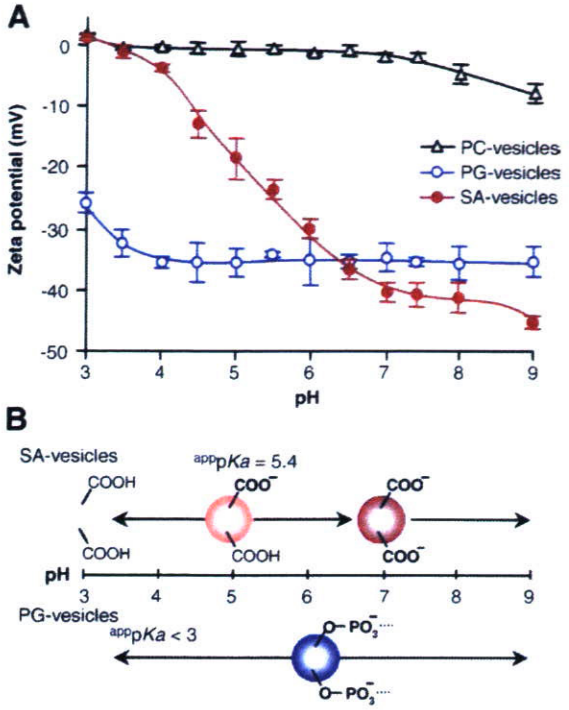

Fig. 3. Ionization state of acidic groups as a function of pH. (A) Zeta potential of vesicles (PC/CH, 1:1, molar ratio) (PC-vesicles), and vesicles containing 9 mol% of SA (SA-vesicles) or PG (PG-vesicles) at various pH. Zeta potentials were measured in 10 mM phosphate buffer (NaCl; 20 mM) at various pH (37 °C). (B) Schematic representation of the ionization state of acidic groups with pH. The apparent pK_as of SA-vesicles and PG-vesicles were calculated to be 5.4 and <3.

This result demonstrated that the capacity of SA as an anionic component of vesicles is equal to acidic phospholipids at pH 7.4.

3.3. Ionization properties of acidic lipids

Stability of the ionization state conferred by acidity is an important characteristic of acidic compounds. We examined the ionization properties of acidic lipids as a function of pH using SA-vesicles and PG-vesicles containing acidic lipids of 9 mol% with zeta potentials of −40.7±2.09 mV and −35.4±0.61 mV (at pH 7.4), respectively. As shown in Fig. 3A, the zeta potential of SA-vesicles varied markedly depending on the environmental pH (pH 3–7). The change in the zeta potential of SA-vesicles is thought to reflect the ionization state of SA, as control vesicles without SA, namely PC-vesicles, maintained almost neutral surfaces irrespective of pH. The relationship between pH and the pK_a of the acid is expressed using the well-known Henderson–Hasselbalch equation as follows:

$$\mathrm{pH} = \mathrm{p}K_a + \log\frac{[-\mathrm{COO}^-]}{[-\mathrm{COOH}]}. \quad (2)$$

When we analyzed the data shown in Fig. 3A using Eq. (2) and the assumption that the zeta potential was linearly correlated with the ionization acid, the pK_a of the carboxyl group of SA was estimated as 5.4 (Fig. 3B). Above pH 7, the zeta potential of SA-vesicles was almost constant, indicating that the carboxyl group of SA would mostly be ionized above pH 7. The zeta potentials of PG-vesicles were almost constant in the range pH 4–9, indicating that the ionized form of the phosphoric acid moiety is stable in this range. The change in the zeta potential observed at a pH lower than pH 4, and its pK_a would be lower than pH 3 [23,24]. Thus, we confirmed that the surface of SA-vesicles and PG-vesicles exhibited the characteristics of a weak acid with SA and a strong acid with PG, respectively, indicating that the individual characteristics of acidic groups are expressed on the surface of vesicles. We also observed that the magnitude of the negative electrostatic charges in SA-vesicles was equal to that observed in PG-vesicles at approximately neutral pH.

3.4. Electrostatic interactivity

Ca^{2+} is found in biological fluids (normally 2–3 mM in plasma) and is known to mediate biological processes by binding to the anionic domains such as those involved in the specific binding of proteins to membranes [25,26]. Acidic phospholipids, such as PG and PS, are also known to bind Ca^{2+} [27–29]. As shown in Fig. 4, the negative charge on anionic vesicles was suppressed by increasing the concentration of Ca^{2+}. When the concentration of Ca^{2+} was increased to 3 mM, the zeta potentials of SA-vesicles and PG-vesicles were −16.4±1.9 mV and −13.8±1.4 mV, respectively. Recently, Hautala et al. reported that vesicles containing phosphatidic acid possess a specifically strong affinity for Ca^{2+}, and that the zeta potential of these vesicles changed from being strongly negative to positive after binding Ca^{2+} [29]. These authors also showed that other acidic phospholipids, including PG, do not exhibit a strong affinity towards becoming cationic. Consequently, one aim of this experiment was to determine whether the binding of Ca^{2+} is a specificity factor between SA-vesicles and PG-vesicles, and also whether the surface of SA-vesicles remained negative in the presence of Ca^{2+}. Our experiment showed that the surface of the SA-vesicles remained

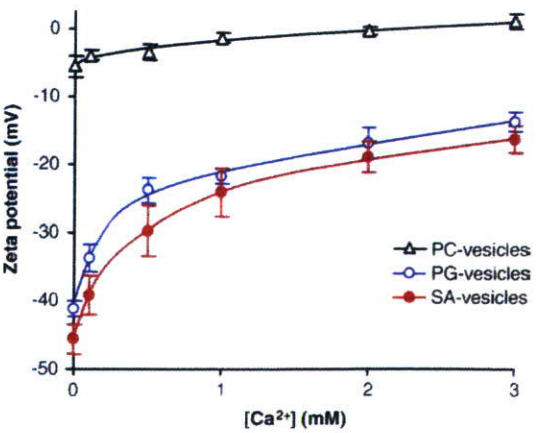

Fig. 4. Change in zeta potential of vesicles as a function of Ca^{2+} concentration. Vesicles were dispersed at 100 μg/mL in 10 mM HEPES buffer (pH 7.4, at 37 °C) containing NaCl and $CaCl_2$ (total: 20 mM). PC-vesicles: PC/ CH (1:1, molar ratio), SA-vesicles: PC/CH/SA (1:1:0.2, molar ratio), and PG-vesicles: PC/CH/PG (1:1:0.2, molar ratio).

Please cite this article as: K. Sou, E. Tsuchida, Electrostatic interactions and complement activation on the surface of phospholipid vesicle containing acidic lipids: Effect of the structure of acidic groups, Biochim. Biophys. Acta (2008), doi:10.1016/j.bbamem.2008.01.006

negative in the presence of Ca^{2+}. In addition, comparisons of SA-vesicles and PG-vesicles also showed that the specificity of binding Ca^{2+} was not observed.

Additional model-based studies of electrostatic interactivity, pentalysine and poly-L-lysine (Mw. 15–30 kDa with a repeating primary lysine amine) were also conducted. Oligomers or polymers of lysine are often used to model basic peptides or macromolecules and their electrostatic interactions on membranes [30,31]. As shown in Fig. 5, the zeta potential is a linear function of the concentration of pentalysine. The lines, which represent the least-squares best fit, have slopes of 9.3 and 7.4 mV per decade for the pentalysine concentrations in SA-vesicles and PG-vesicles. The slope for PC-vesicles was as little as 0.26 mV per decade of pentalysine concentration (data not shown), indicating that the negative charge of acidic lipids mediate the interaction with basic pentalysine. A change in the zeta potential is due to binding of basic peptide [31] and a similar decay slope of the zeta potential would indicate that the binding constant of a basic peptide to SA-vesicles and PG-vesicles was similar. As shown in Fig. 6, the change in the zeta potential of these vesicles due to the interaction with poly-L-lysine increased drastically, changing from a negative to a positive in presence of 1.5–2 μg/mL poly-L-lysine. Conversely, the change in the surface potential of PC-vesicles was negligible, indicating that the acidic lipids mediate the interaction with basic macromolecules. This experiment also demonstrates that the interactivity of SA-vesicles and PG-vesicles to basic macromolecules is equal at pH 7.4, and that within an electrostatic context, SA-vesicles and PG-vesicles interact similarly with basic compounds at physiological pH. It has been shown that electrostatic interactions are involved in the binding of C1q to the surface of anionic vesicles containing acidic phospholipid [6]. In the event that the negative charge on the surface of vesicles is critical for complement activation, both the SA-vesicles and PG-vesicles should be capable of activating the complement system to similar degree. We therefore conducted animal experiments to clarify the issue of complement activation by the anionic electrostatic charge of vesicles.

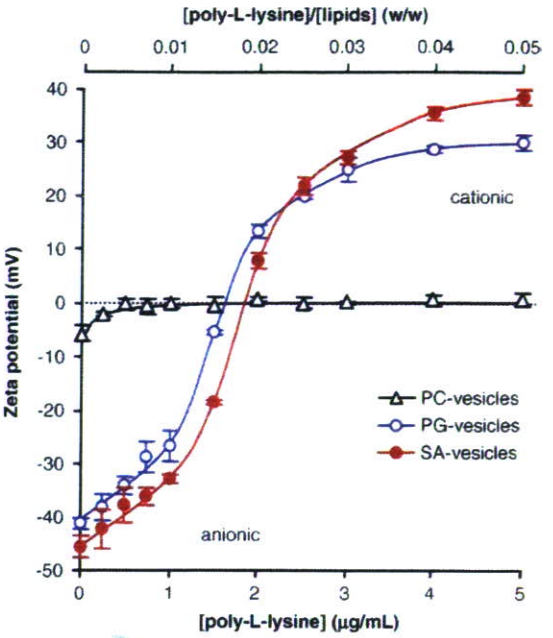

Fig. 6. Change in zeta potential of vesicles as a function of the concentration of basic macromolecule (poly-L-lysine, Mw. 15–30 kDa). Vesicles were dispersed at 100 μg/mL in 10 mM HEPES buffer (pH 7.4, at 37 °C, NaCl, 20 mM) containing various amount of poly-L-lysine. PC-vesicles: PC/CH (1:1, molar ratio), SA-vesicles: PC/CH/SA (1:1:0.2, molar ratio), and PG-vesicles: PC/CH/PG (1:1:0.2, molar ratio).

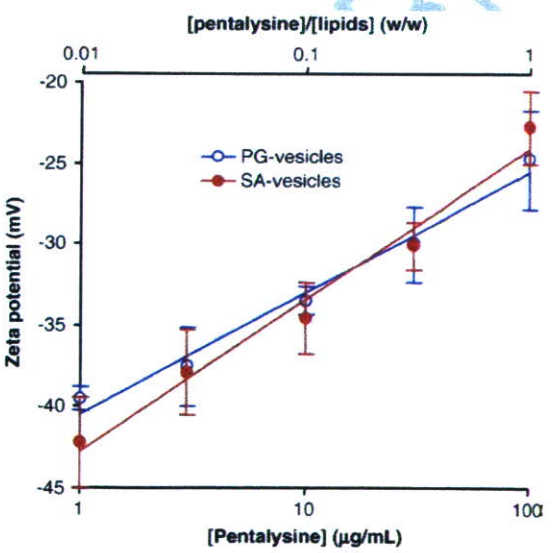

Fig. 5. Change in zeta potential of vesicles as a function of the concentration of basic oligomer (pentalysine). Vesicles were dispersed at 100 μg/mL in 10 mM HEPES buffer (pH 7.4, at 37 °C, NaCl, 20 mM) containing various amount of pentalysine. The lines have slopes of 9.3 and 7.4 mV per decade for the pentalysine concentrations in SA-vesicles and PG-vesicles. SA-vesicles: PC/CH/SA (1:1:0.2, molar ratio) and PG-vesicles: PC/CH/PG (1:1:0.2, molar ratio).

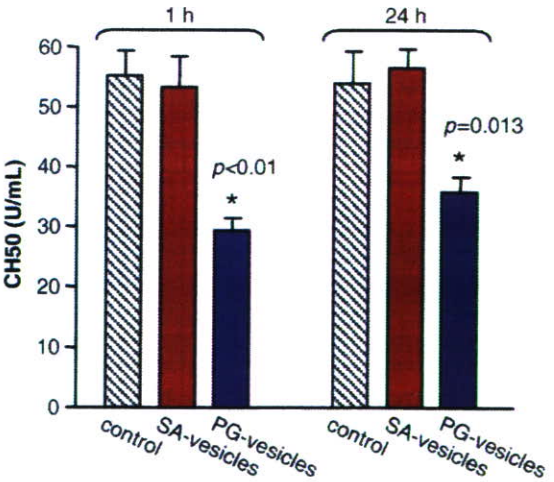

Fig. 7. Comparison of the 50% hemolytic unit of complement (CH50) in rat serum at 1 or 24 h after infusion of saline (control), SA-vesicles, or PG-vesicles. CH50 value for PG-vesicles was significantly lower than that of the control ($p<0.01$ at 1 h, $p=0.013$ at 24 h), indicating the complement consumption in serum after activation. Equal CH50 value for SA-vesicles with the control indicates that SA-vesicles failed to activate complement.

Please cite this article as: K. Sou, E. Tsuchida, Electrostatic interactions and complement activation on the surface of phospholipid vesicle containing acidic lipids: Effect of the structure of acidic groups, Biochim. Biophys. Acta (2008), doi:10.1016/j.bbamem.2008.01.006

3.5. Complement activation

Serum was collected at 1 and 24 h after the infusion of SA-vesicles or PG-vesicles in experimental rats to determine CH50 levels. The control group received saline as a vehicle. The values of CH50 in control rats, and SA-vesicles- and PG-vesicles-administered rats, were 55.1±4.1 U/mL, 53.2±4.8 U/mL, and 29.3±1.6 U/mL at 1 h after infusion of sample, respectively. At 24 h, the values of CH50 in control rats, and SA-vesicles- and PG-vesicles-administered rats, were 54.0±4.7 U/mL, 56.5±3.3 U/mL, and 35.8±2.3 U/mL, respectively (Fig. 7). The lower CH50 levels observed in the PG-vesicles-administered group in comparison with the control group indicate that complement consumption occurred after activation. These findings imply that significant complement activation is induced in rats receiving PG-vesicles compared to the control group ($p<0.01$ at 1 h, $p=0.013$ at 24 h). Complement consumption was not observed in rats administered SA-vesicles.

Since the negative charge and electrostatic interactivity of SA-vesicles were the same as in PG-vesicles (Figs. 2–6), the data obtained from the animal experiments indicates that the negative charge on the anionic vesicle is not a critical factor underlying the activation of complement. The first step in the activation of the classical complement pathway involves the binding of an activator to C1q, resulting in the activation of serine proteases C1r and C1s. It has been suggested that the negative charge of an activator such as PG-vesicles is involved in some way with the binding of the activator to C1q [1–8]. Assuming that the electrostatic interaction is non-specific, SA-vesicles should interact with C1q electrostatically. Since the action of complement proteases, which follows the binding of the activator to the C1q, is known to be highly specific [32,33], it seems likely that complement activation on anionic surface is limited to an activation step rather than a binding step. Such specific activation of complement by the anionic vesicles in the present study may be involved in the physiological regulation of complement activation on anionic biomembranes.

4. Conclusions

The carboxylic acid of SA and phosphoric acid of PG have equal capacity as anionic components of vesicles at neutral pH. The results presented in this investigation demonstrated that the negative electrostatic charge of anionic vesicles is not a critical factor in the activation of complement. Rather, the induction of complement activation by anionic vesicles is dependent on the structure of acidic lipids. This finding may facilitate development and various biological applications of anionic vesicles.

Acknowledgements

This work was partly supported by Health Sciences Research Grants (Research on Regulatory Science); the Ministry of Health, Labour and Welfare, Japan, and the Ministry of Education, Science, Sports and Culture, Grant-in-Aid for Scientific Research (B), 17300162. The authors gratefully acknowledge Dr. K. Kobayashi and Dr. H Horinouchi (Keio University) for their support in the animal experiments, Dr. M. Suematsu (Keio University) for an important suggestion on bioactivity of anionic vesicles, and Dr. S. Takeoka and Dr. H. Sakai (Waseda University) for advice and discussions related to this research.

References

[1] H.C. Loughrey, M.B. Bally, L.M. Reinish, P.R. Cullis, The binding of phosphatidylglycerol liposomes to rat platelets is mediated by complement, Thromb. Haemost. 64 (1990) 172–176.

[2] A. Chonn, P.R. Cullis, D.V. Devine, The role of surface charge in the activation of the classical and alternative pathways of complement by liposomes, J. Immunol. 146 (1991) 4234–4241.

[3] J. Szebeni, The interaction of liposomes with the complement system, Crit. Rev. Ther. Drug Carr. Syst. 15 (1998) 57–88.

[4] S.M. Moghimi, I. Hamad, N.L. Andresen, K. Jorgensen, J. Szebeni, Methylation of the phosphate oxygen moiety of phospholipid-methoxy (polyethylene glycol) conjugate prevents PEGylated liposome-mediated complement activation and anaphylatoxin production, FASEB J. 20 (2006) 2591–2593.

[5] A.J. Bradley, D.E. Brooks, R. Norris-Jones, D.V. Devine, C1q binding to liposomes is surface charge dependent and is inhibited by peptides consisting of residues 14–26 of the human C1qA chain in a sequence independent manner, Biochim. Biophys. Acta 1418 (1999) 19–30.

[6] A.J. Bradley, E. Maurer-Spurej, D.E. Brooks, D.V. Devine, Unusual electrostatic effects on binding of C1q to anionic liposomes: role of anionic phospholipid domains and their line tension, Biochemistry 38 (1999) 8112.

[7] H. Jiang, B. Cooper, F.A. Robey, H. Gewurz, DNA binds and activates complement via residues 14–26 of the human C1q A chain, J. Biol. Chem. 267 (1992) 25597–25601.

[8] H. Jiang, D. Burdick, C.G. Glabe, C.W. Cotman, A.J. Tenner, beta-Amyloid activates complement by binding to a specific region of the collagen-like domain of the C1q A chain, J. Immunol. 152 (1994) 5050–5059.

[9] A.J. Bradley, D.V. Devine, S.M. Ansell, J. Janzen, D.E. Brooks, Inhibition of liposome-induced complement activation by incorporated poly(ethylene glycol)-lipids, Arch. Biochem. Biophys. 357 (1998) 185–194.

[10] E. Tsuchida (Ed.), Substitute: Present and Future Perspective, Elsevier Science, Amsterdam, 1998.

[11] S. Takeoka, T. Ohgushi, K. Terase, T. Ohmori, E. Tsuchida, Layer-controlled hemoglobin vesicles by interaction of hemoglobin with a phospholipid assembly, Langmuir 12 (1996) 1755–1759.

[12] H. Sakai, K. Hamada, S. Takeoka, H. Nishide, E. Tsuchida, Physical properties of hemoglobin vesicles as red cell substitutes, Biotechnol Prog. 12 (1996) 119–125.

[13] K. Sou, Y. Naito, T. Endo, S. Takeoka, E. Tsuchida, Effective encapsulation of proteins into size-controlled phospholipid vesicles using freeze-thawing and extrusion, Biotechnol Prog. 19 (2003) 1547–1552.

[14] H. Sakai, H. Horinouchi, M. Yamamoto, E. Ikeda, S. Takeoka, M. Takaori, E. Tsuchida, K. Kobayashi, Acute 40 percent exchange-transfusion with hemoglobin-vesicles (HbV) suspended in recombinant human serum albumin solution: degradation of HbV and erythropoiesis in a rat spleen for 2 weeks, Transfusion 46 (2006) 339–347.

[15] H. Saka i, Y. Masada, H. Horinouchi, E. Ikada, K. Sou, S. Takeoka, M. Suematsu, M. Takaori, K. Kobayashi, E. Tsuchida, Physiological capacity of the reticuloendothelial system for the degradation of hemoglobin vesicles (artificial oxygen carriers) after massive intravenous doses by daily repeated infusions for 14 days, J. Pharmacol. Exp. Ther. 311 (2004) 874–884.

[16] K. Sou, R. Klipper, B. Goins, E. Tsuchida, W.T. Phillips, Circulation kinetics and organ distribution of Hb-vesicles developed as a red blood cell substitute, J. Pharmacol. Exp. Ther. 312 (2005) 702–709.

[17] H. Abe, M. Fujihara, H. Azuma, H. Ikeda, K. Ikebuchi, S. Takeoka, E. Tsuchida, H. Harashima, Interaction of hemoglobin vesicles, a cellular-type artificial oxygen carrier, with human plasma: effects on coagulation, kallikrein-kinin, and complement systems, Artif. Cells Blood Substit. Biotechnol. 34 (2006) 1–10.